iScience

Article

ATP8A1-translocated endosomal phosphatidylserine fine-tunes the multivesicular body formation and the endo-lysosomal traffic

Graphical abstract

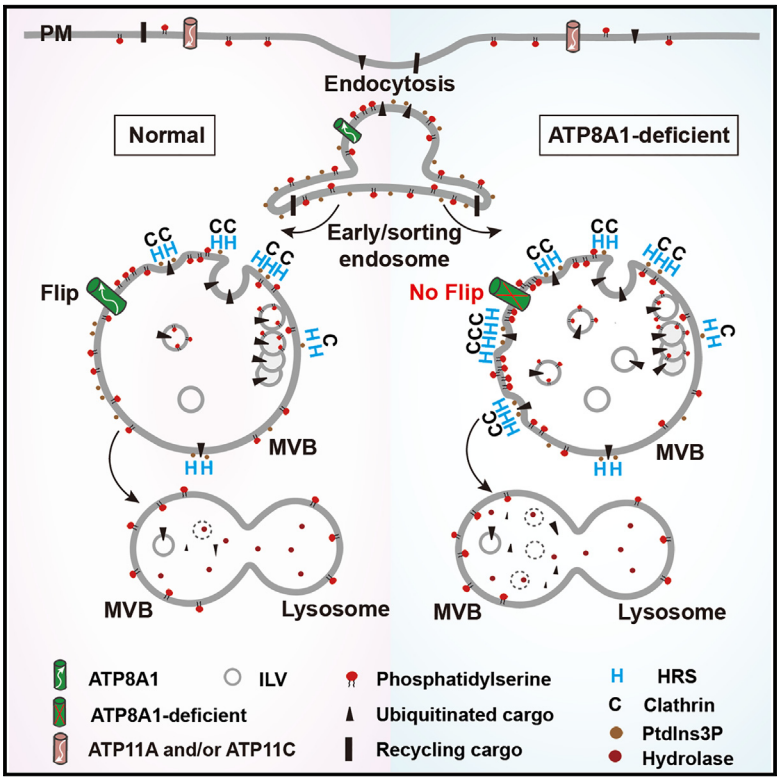

Highlights

- ATP8A1, a phosphatidylserine flippase, is highly enriched in late endosomes
- Loss of ATP8A1 promotes the lysosome-destined transport
- ATP8A1 loss leads to PS loading in the luminal leaflet of MVB′s limiting membrane
- Loss of ATP8A1 fine-tunes ILVs initiation and ESCRT components recruitment

Authors

Zengmei Lan, Yangli Tian, Chengang Li, Yudong Wang, Ping Yi, Rongying Zhang

Correspondence

ryzhang@hust.edu.cn

In brief

Biological sciences; Cell biology; Organizational aspects of cell biology; Functional aspects of cell biology

Lan et al., 2025, iScience *28*, 111973
March 21, 2025
https://doi.org/10.1016/j.isci.2025.111973

CellPress

iScience

CellPress
OPEN ACCESS

Article

ATP8A1-translocated endosomal phosphatidylserine fine-tunes the multivesicular body formation and the endo-lysosomal traffic

Zengmei Lan,[1,3] Yangli Tian,[1,2,3] Chengang Li,[1] Yudong Wang,[1] Ping Yi,[1] and Rongying Zhang[1,4,*]

[1]Key Laboratory of Molecular Biophysics of the Ministry of Education, College of Life Science and Technology, Huazhong University of Science and Technology, Wuhan, Hubei, China

[2]Hebei Key Laboratory of Medical Data Science, School of Medicine, Hebei University of Engineering, Handan, China

[3]These authors contributed equally

[4]Lead contact

*Correspondence: ryzhang@hust.edu.cn

https://doi.org/10.1016/j.isci.2025.111973

SUMMARY

P4-ATPases are phospholipid flippases responsible for the transbilayer lipid asymmetry. ATP8A1, a P4-ATPase family member, has been reported to be involved in phosphatidylserine (PS) translocation at the *trans*-Golgi network, early endosomes and recycling endosomes. However, the possible roles of the PS on late endosomes/lysosomes pathway and how they are regulated remain to be elucidated. This study showed enrichment of ATP8A1 in Rab7-positive late endosomal compartments, and that ATP8A1 primarily flips the endosomal PS from the luminal leaflet to the cytosolic leaflet but not the PS in the inner leaflet of the plasma membrane. ATP8A1 depletion accelerates the lysosome-destined cargo proteins transfer into the intraluminal vesicles (ILVs) of multivesicular bodies (MVBs) and alters the signaling of epidermal growth factor receptor. Mechanistically, ATP8A1 depletion leads to PS loading in the luminal leaflet of MVB's limiting membrane, which fine-tunes ILVs initiation and endosomal sorting complex required for transport (ESCRT) component recruitment.

INTRODUCTION

Phosphatidylserine (PS), a relatively minor constituent of biological membrane, is enriched in the inner leaflet of the plasma membrane (PM) and facilitates various signaling events.[1–3] PS is also highly enriched in the cytoplasmic leaflet of recycling endosomes (REs) whereby not only participates in membrane traffic from REs to PM or to the Golgi, but also shown to regulate the Yes-associated protein (YAP)-dependent transcription and cell proliferation.[2,4–6] However, a minor but detectable amount of PS localizes on the late endosomes (LEs) and lysosomes,[7–9] where its function has been less well defined.[3] Indeed, the precise localization and the dynamics of PS within whole and live cells remains an area of active research.

The transbilayer lipid asymmetry is generated and regulated by lipid flippases, floppases, and scramblases. P4-ATPases are phospholipid flippases that translocate cell membrane phospholipids from the exoplasmic/luminal leaflet to the cytoplasmic leaflet to generate and maintain membrane lipid asymmetry; deficiencies of which are associated with human diseases, including neurological dysfunction, liver disorders, immune deficiency, and reduced fertility.[10] Mammalian P4-ATPases exhibit strict substrate specificities, till recently five (ATP8A1, 8A2, 11A, 11B, and 11C) out of fourteen human P4-ATPase members have been identified to possess PS flippase activity.[1] Recent work has proposed two models for the involvement of PS flippases in the vesicle formation among the PM, endosomes and the Golgi: (1) PS plays a vital role in the process, for which there are further two possibilities. One is PS level on the cytosolic side of PM or endosomes determines the recruitment of PS-binding proteins to trigger membrane budding, which promotes subsequent vesicle fission and transport.[2,11,12] The other one is PS flipping to the cytoplasmic leaflet creates an imbalance in surface area between the leaflets, which imparts molecular crowding stress on the cytosolic leaflet and a packing defect stress on the exoplasmic leaflet, thereafter induces membrane bending that supports vesicle budding.[12] (2) PS is not directly involved into the process; however, flippase on own works directly with the vesicle budding machinery to generate positive curvature at the site of vesicle formation. For instance, though the substrate is undefined, ATP9A was found to activate Rab5 and Rab11 to promote the endosomal recycling pathway in neural cells.[13]

Among the five human PS flippases, only ATP8A1, 8A2, and ATP11B localizes at internal membranes, such as endosomes and the *trans*-Golgi network (TGN).[14] Pieces of evidence suggest that ATP8A1, its *C. elegans* homologue TAT-1, and its tissue-specific paralog ATP8A2 play a pivotal role in endocytic recycling by recruiting EHD1/RME-1 to help drive scission of tubular carriers.[2] However, ATP8A1 has been shown various subcellular

localizations in different cell types; for example, it localizes to REs in COS-1 cells and to the PM in CHO-K1 cells, while mainly localizes to LEs/lysosomes in HeLa cells.[2,15–18] A recent study in surfactant-producing alveolar type 2 (AT2) cells of the distal lung epithelium uncovered that ATP8A1 localizes to lamellar bodies, the lysosome-related organelles; moreover, mis-sorting of ATP8A1 to the early sorting and/or recycling endosomes promotes toxic activation of YAP, augmenting cell migration and AT2 cell numbers.[19] In all, mounting evidence supports that P4-ATPases regulate transbilayer lipid dynamics for specialized cellular processes by functioning where they predominantly localize. However, till now the functional knowledge of late endosomal compartments-localized PS and the associated flippase are still lacking.

Multivesicular bodies (MVBs) are key intermediates in endolysosomal transport, which are formed by the invagination and scission of buds from the limiting membrane of the endosome into the lumen. Apart from phosphatidylinositide phosphates (PIPs), it is still unclear whether and how the other anionic phospholipids, like lysobisphosphatidic acid (LBPA) and PS, are involved in MVBs generation.[20,21] This study was designed to explore the roles of endosomal PS flippase ATP8A1 in the control of trafficking pathways with special emphasis on LEs-lysosome function. The key findings presented here identified endosomal PS transbilayer translocation by ATP8A1, which plays a role in late endosomal transportation destined to degradative lysosomes. Detailed mechanistic investigation revealed that ATP8A1-mediated PS translocation modulates the PS content between the transbilayers of MVBs and contributes to the MVBs formation, which ultimately affects the turnover kinetics of signaling receptor EGFR. This newly recognized connection between ATP8A1, endosomal PS, and MVBs uncovers a molecular sequence by which P4-ATPases can be linked to regulation of endosomal transportation along the LEs-lysosomal pathway and may help us understand how transbilayer PS content tunes membrane bending and vesicle budding.

RESULTS

P4-ATPase member ATP8A1 shows highest enrichment in Rab7-positive compartments

P4-ATPase member ATP8A1 is composed of 10 transmembrane helices with its N-/C-terminus both in the cytoplasm. Endogenous ATP8A1 immuno-labeling is notoriously difficult due in part to the paucity of highly specific and sensitive antibodies,[22] and most studies describing ATP8A1 traffic pathway have to rely on use of the ATP8A1 fusion protein. CDC50 protein is required for most P4-ATPases exit from the endoplasmic reticulum (ER) and target to the cellular compartments or the PM.[1,23] Our preliminary experiments indicated that when expressed at low level in HeLa cells, EGFP-tagged ATP8A1 is able to normally exit from the ER facilitated by the endogenous CDC50A (Figures S1A–S1C); by contrast, in COS-7 cells, co-expression of CDC50A is required for tagged ATP8A1 exiting from the ER[24] (Figures S1D and S1E). These results are in line with previous studies that, endogenous CDC50 seems sufficient to translocate exogenously expressed P4-ATPases from the ER, at least in some cell types.[15,17]

Flow cytometry analysis was then used to assess the proportion of ATP8A1 expressed on the cell surface in HeLa cells (Figure 1A). The median fluorescence intensity (MFI) of permeabilized samples, which indicates the total protein expression level, was compared with the MFI of surface staining, and the result indicated that the majority of ATP8A1 is in the cytoplasm, consistent with previous studies.[14,17] We further examined the distribution of EGFP-ATP8A1 in membrane compartments on both the endocytic and the secretory pathways. Small EGFP-ATP8A1 puncta were dispersed in the cytoplasm and co-localized with Rab5-positive early endosomes (EEs), Rab11-positive REs, Rab7-positive LEs, and lysotracker-positive lysosomes (Figure 1B). Nevertheless, only a small proportion was localized on the Golgi and almost no localization was observed in ER (Figure 1B). Surprisingly, quantitative analysis showed that LEs possess the highest EGFP-ATP8A1 content (Figures 1C and 1D). TRITC-wheat germ agglutinin (WGA) was used to label the PM, in line with the flow cytometry analysis, only a very small amount of EGFP-ATP8A1 localizes to the PM (Figures 1B and 1C).

Collectively, these data indicated that when expressed at low level, EGFP-tagged ATP8A1 is appropriately folded and normally exit from the ER facilitated by the endogenous CDC50A. Moreover, the steady-state ATP8A1 mainly localizes to the endosomal compartments with a tendency to enrich on the LEs as well as the REs.

ATP8A1 primarily flips the endosomal PS from the luminal leaflet to the cytosolic leaflet

Next, we examined the function of PS flipping for ATP8A1 (Figure 2). A fusion of the C2 domain of lactadherin (Lact-C2) with fluorescent protein was used to visualize PS on the cytoplasmic membrane leaflet, which cannot probe PS on the exoplasmic/luminal membrane leaflet.[8] When expressed in HeLa cells, GFP/mCherry-Lact-C2 decorates the cell periphery as well as internal organelles (Figures 2A and S2A, top row). Pearson's coefficient analysis for GFP-Lact-C2 with various subcellular compartments demonstrated that, besides the inner leaflet of PM, PS is mainly enriched in REs and EEs with a relatively small proportion in LEs and almost no localization on the cytoplasmic leaflets of ER or Golgi (Figure S2B), which is consistent with previous studies.[2,4,5,8,9] In cells knockdown of ATP8A1, the amount of cytosolic mCherry-Lact-C2 puncta decreased by 59.34% with the fluorescence intensity (FI) decreased by 48.77% (Figures 2A–2C); further colocalization analysis showed concomitant PS reduction in the cytoplasmic leaflet of EEs, REs, and LEs (Figures S2C–S2F). In contrast, FI of PM-associated Lact-C2 was not markedly affected (Figures 2A, insets 2 and 4; 2D), indicating that knockdown of ATP8A1 reduced PS in the cytoplasmic leaflet of endosomes but not that in the inner leaflet of the PM.

The dominant negative mutant ATP8A1D409N was also used to provide parallel evidence for how ATP8A1 affects the PM and endosomal PS asymmetry (Figures 2E–2H). As seen, the cytoplasmic mCherry-Lact-C2 puncta significantly decreased in EGFP-ATP8A1D409N-expressing cells, strongly in contrast to the neighboring D409N-negative expressing cells, while the PM-associated Lact-C2 was not changed profoundly. The phosphorylation-site mutant D409N is known to sequester CDC50,

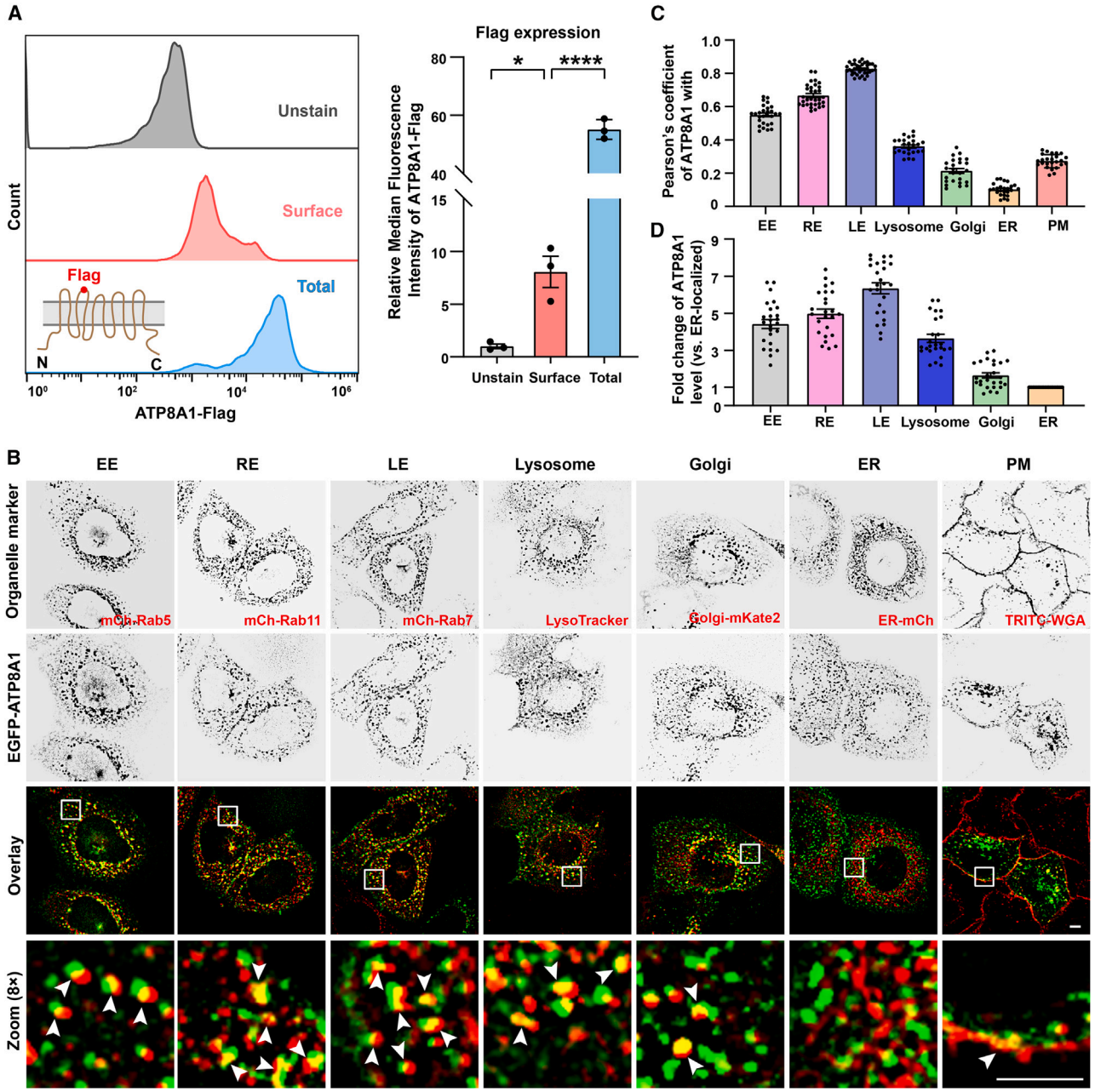

Figure 1. ATP8A1 shows the highest enrichment in Rab7-positive compartments

(A) Representative stacked histograms show the flow cytometry-based analysis of total and surface pool of ATP8A1 in ATP8A1-Flag-stably expressing HeLa cells. Cells with or without permeabilization were stained with anti-FLAG antibody, and unstained sample was used as the negative control. Insert illustrates the construct of ATP8A1-Flag, in which FLAG tag was inserted within the 2nd extracellular loop. The graph represents the relative median fluorescence intensity for ATP8A1-Flag calculated. *$p < 0.05$; ****$p < 0.0001$ by one-way ANOVA with Tukey's post hoc test. Data are expressed as mean ± SD, $N = 3$ from three independent experiments.

(B) Confocal micrographs showing the localization of EGFP-ATP8A1 with respect to the fluorescent organelle markers. Rab5, Rab11, and Rab7 were used for early endosome, recycling endosome and late endosome, respectively. Plasma membrane (PM) was stained by TRITC-WGA. The arrowheads in the magnified images mark the overlapped pixels. Scale bar, 5 μm.

(C) Quantification of the Pearson's correlation coefficient for the co-localization of EGFP-ATP8A1 with different organelle markers from B. Data are displayed as mean ± SEM, $N \geq 25$ cells from three independent experiments.

(D) Fold change of EGFP-ATP8A1 level in each endomembrane compartment. The amount of EGFP-ATP8A1 puncta positive for individual fluorescent organelle in B was quantified, and ER-localized EGFP-ATP8A1 level was normalized as 1. Data are displayed as mean ± SEM, $N \geq 25$ cells from three independent experiments.

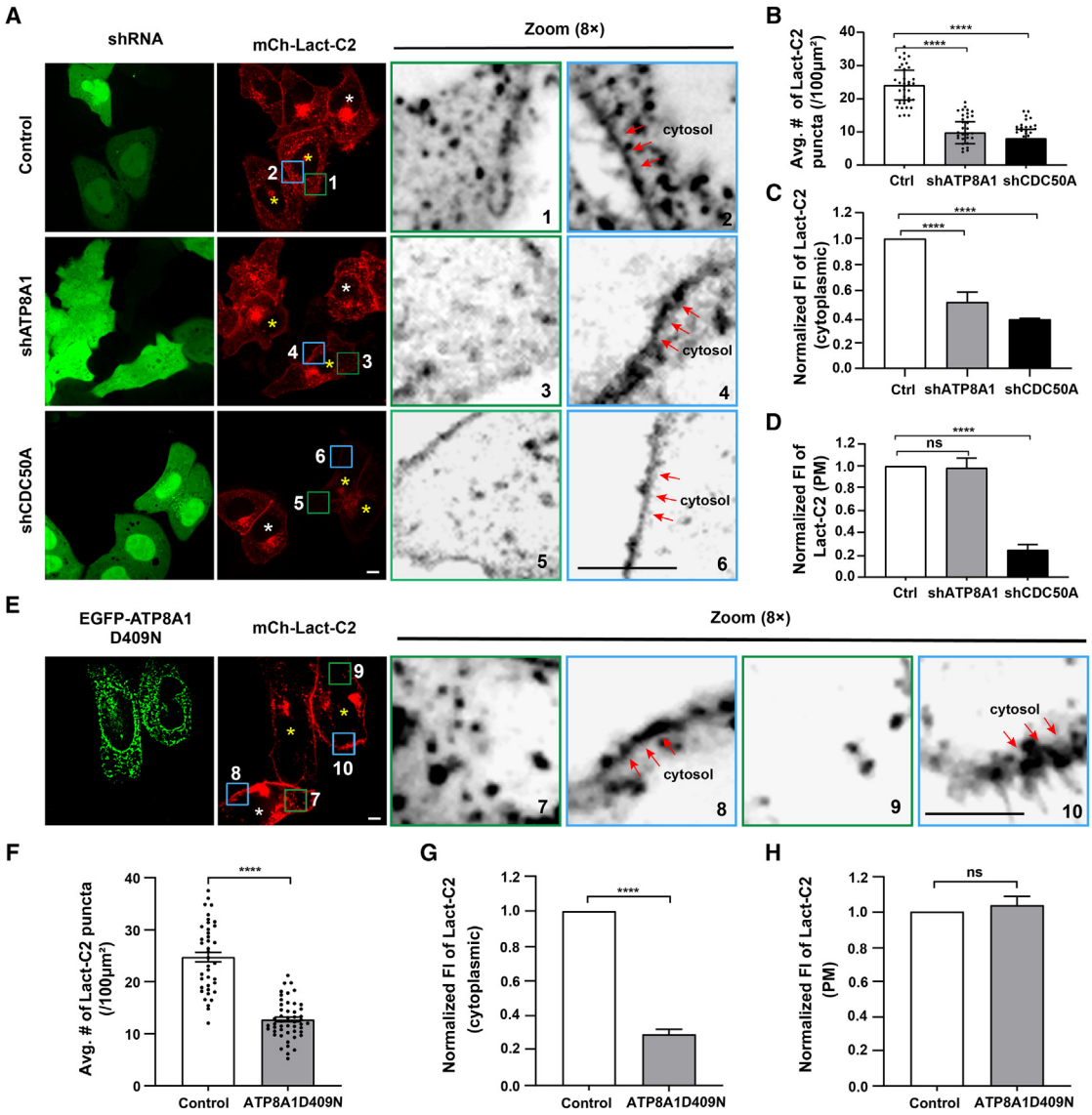

Figure 2. ATP8A1 primarily flips the endosomal PS from the luminal leaflet to the cytosolic leaflet

(A) Confocal micrographs showing the PM- and cytosolic-localized mCherry-Lact-C2 in sh-control, sh-ATP8A1, and sh-CDC50A HeLa cells, respectively. Scale bar, 5 μm.

(B–D) Quantification of the puncta number (B) and normalized fluorescence intensity (FI) of the cytoplasmic mCherry-Lact-C2 (C) and PM mCherry-Lact-C2 (D) for each condition indicated in A. Statistical analysis was performed using Brown-Forsythe and Welch ANOVA with Dunnett T3 multiple comparison test (mean ± SEM) in B, and one-way ANOVA with Dunnett's post hoc test (mean ± SD) in C and D. N ≥ 30 cells from three independent experiments. ****$p < 0.0001$; ns = non-significant.

(E) Confocal micrographs showing the PM- and cytoplasmic-localized mCherry-Lact-C2 in EGFP-ATP8A1 D409N-expressing cells. Scale bar, 5 μm.

(F–H) Quantification of the puncta number (F) and normalized FI of the cytoplasmic mCherry-Lact-C2 (G) and PM mCherry-Lact-C2 (H) in E. ****$p < 0.0001$; ns = non-significant by unpaired *t* test with Welch's correction (mean ± SEM) in F, or unpaired two-tailed Student's t test (mean ± SD) in G and H. N ≥ 30 cells from three independent experiments. In A and E, yellow or white asterisk depicts shRNA-positive or -negative cells. Green and blue boxes were zoomed in to depict intracellular and PM Lact-C2 signals, respectively. The arrows indicate PM.

which prevents ATP8A1 from leaving the ER.[16,25] These data indicated that the ER retention of ATP8A1 also leads to abnormal endosomal sideness of PS, but has no prominent effect on the PM-associated PS in HeLa cells.

To rule out imbalance of endosomal PS caused by the vesicular transport blockage, we examined the effect of ATP8A1 depletion on the endocytic pathway. Transferrin (Tfn) is a canonical cargo internalized by clathrin-mediated endocytosis; after delivery of iron in EEs, Tfn receptor (TfR) bound Tfn further recycles out from REs into the extracellular environment.[26] Brief incubation with Alexa 568-Tfn produced comparable cytoplasmic fluorescence in cells with/without ATP8A1 (Figures S3A and

S3B), indicating membrane flow from the PM to the endosomes is not impaired by ATP8A1 deficiency. Moreover, chase for various time periods showed that the internalized Alexa 568-Tfn in the cytoplasm is decayed obviously slower in ATP8A1 deficient cells than in control cells (Figures S3A and S3B), supporting impaired recycling by ATP8A1 knockdown, as previously revealed in COS-1 cells.[2] Take into account of the endo-lysosomal localization of PS (Figure S2), we further wondered if disturbance of ATP8A1 brought any morphology or distribution alteration to the endosomal compartments. TfR and LAMP1 were used to trace the endosomes on the recycling pathway and the degradation compartments including both LEs and lysosomes, respectively.[7] No visible changes were observed for the amount, size or distribution of these markers in the cytoplasm of ATP8A1D409N-transfected cells (Figures S3C–S3F), indicating that the endosomal pools are integral in the context of ATP8A1 loss-of-function.

As a control, we further examined the impact of CDC50A knockdown on mCherry-Lact-C2. As seen (Figures 2A–2D), shRNA-mediated CDC50A knockdown led to reduction of both PM and endosomal Lact-C2. Annexin V, a non-permeable PS-binding protein that only binds to cells when PS is displayed in the outer PM leaflet, was also used to evaluate PS externalization caused by ATP8A1 depletion. As seen, either ATP11A or ATP11C depletion showed markedly higher externalization of PM-associated PS than ATP8A1 depletion, in concert with previous studies that ATP11A and ATP11C are major PM-localized PS flippases in many cell types (Figures S2G and S2H).[1,14,27] Together, these data indicated that the primary role of ATP8A1 is to flip the endosomal PS from the luminal leaflet to the cytoplasmic leaflet and has minor effect on the PS asymmetry of PM in HeLa cells.

Loss of ATP8A1 enhances degradation of the endo-lysosomal cargo EGFR

The prominent enrichment of ATP8A1 on the LEs prompted us to explore the involvement of ATP8A1 in the endocytic degradation pathway. To this end, the degradation of EGFR was evaluated. In shATP8A1 stably expressing cells, the steady-state protein level of EGFR was determined to be lower than in control cells (Figures S4A–S4C). To further examine the effect on the ligand-mediated EGFR trafficking and turnover, control or shATP8A1 stable cell lines were treated with EGF (in the presence of cycloheximide to block *de novo* protein synthesis) for the indicated time, and EGFR abundance was monitored by western blot and quantified (Figures 3A and 3B). As seen, the extent of EGFR degradation was enhanced by about 1.96-, 1.18-, and 0.67-fold, respectively, after EGF-treatment of 15 min, 30 min, and 60 min in shATP8A1 cells (Figure 3B). Moreover, this degradation was effectively reversed by BafA1 treatment (Figures 3C and 3D), supporting that albeit the kinetics is altered, EGFR degradation still occurs in lysosomes of ATP8A1-depleting cells. Conversely, elevated ATP8A1 expression delayed the post-endocytic degradation of cell-surface-labelled EGFR (Figures 3E and 3F). In HA-ATP8A1-overexpressing cells, the extent of EGFR degradation was decreased to 45.73%, 52.42%, and 71.26% of that for the control cells upon EGF treatment of 15, 30, and 60 min, respectively. Taken together, these data indicated that ATP8A1 negatively regulates ligand-dependent lysosomal degradation of EGFR.

We also evaluated whether EGFR signaling is altered by ATP8A1 depletion. Our results indicated that AKT activation kinetics was prominently changed, with activation increased at early time points but deactivated to the basal level soon at later time points; while ERK phosphorylation was only marginally impacted by the knockdown of ATP8A1 (Figures S4D–S4F).

Blocking cytoplasmic facial endosomal PS promotes EGF-induced EGFR degradation

Our previous results and other groups revealed that the principle functional consequence of ATP8A1 is to maintain the endosomal PS asymmetry. Next, we wonder whether ATP8A1 control of the EGFR transportation is related to the endosomal PS translocation. According to previous studies, overexpression of PS-specific probes will block/mask PS and interfere with the recruitment of PS-binding proteins.[4,5] Evectin-2-derived PH (2×PH) was identified to bind specifically to PS on the endomembrane but less in the PM than Lact-C2.[28] In line with this, we determined that 2×PH bound to the cytoplasmic leaflets of the endocytic organelles, including EEs, REs and LEs/lysosomes, but less targeted to the PM in HeLa cells (Figures 4A and 4B). Using overexpressed 2×PH to block endosomal PS but not PM-associated PS, we then observed EGF-induced EGFR degradation. As seen, following EGF pulse for various periods, EGFR was degraded prominently faster in 2×PH-expressing cells compared with the neighboring vehicle cells (Figures 4C and 4D). These data indicated that the cytoplasmic faced endosomal PS is involved in the regulation of transportation destined for lysosomes.

ATP8A1 tunes EGFR sorting into the ILVs of MVBs

We then sought to identify the intracellular compartment where ATP8A1 regulates EGFR degradation and the underlying mechanism. Following EGF-stimulated internalization in EEs, EGFRs are transferred from the limiting membrane to the intraluminal vesicles (ILVs) of MVBs.[29] We thus examined whether ATP8A1 altered the sorting of EGFR into ILVs. To this end, we took advantage of the enlarged endosomes produced by expressing Rab5Q79L, a constitutively active Rab5 mutant, to better visualize the EGF-dependent sorting and transfer of EGFR from the limiting membrane into ILVs[30,31] (Figure 5). Cell-surface EGFRs were labeled with Alexa Fluor 555-EGF and internalized for various time periods.[32]

As seen, Alexa 555-EGF showed prominent localization on the limiting membrane of enlarged endosomes 15 min post-internalization, with only about 9.06% endosomes exhibiting intraluminal fluorescence (Figures 5A and 5B); whereas internalization for 30 min led to EGF filling in the ILVs of ca. 63.20% enlarged endosomes, and 60 min further increased EGF loading in ca. 75.46% of enlarged endosomes (Figures 5A and 5B). In contrast, after internalization for 15 min, ca. 74.83% of enlarged endosomes were filled with Alexa 555-EGF in ATP8A1-depleted cells (Figures 5C and 5D). The EGF distribution across the MVBs was quantified by line scan analysis of confocal cross-sections as previously described.[33] A representative line scan analysis of an endosome is shown in Figure 5E. The normalized locations of 0 and 100 indicate the limiting membrane, and the hatched

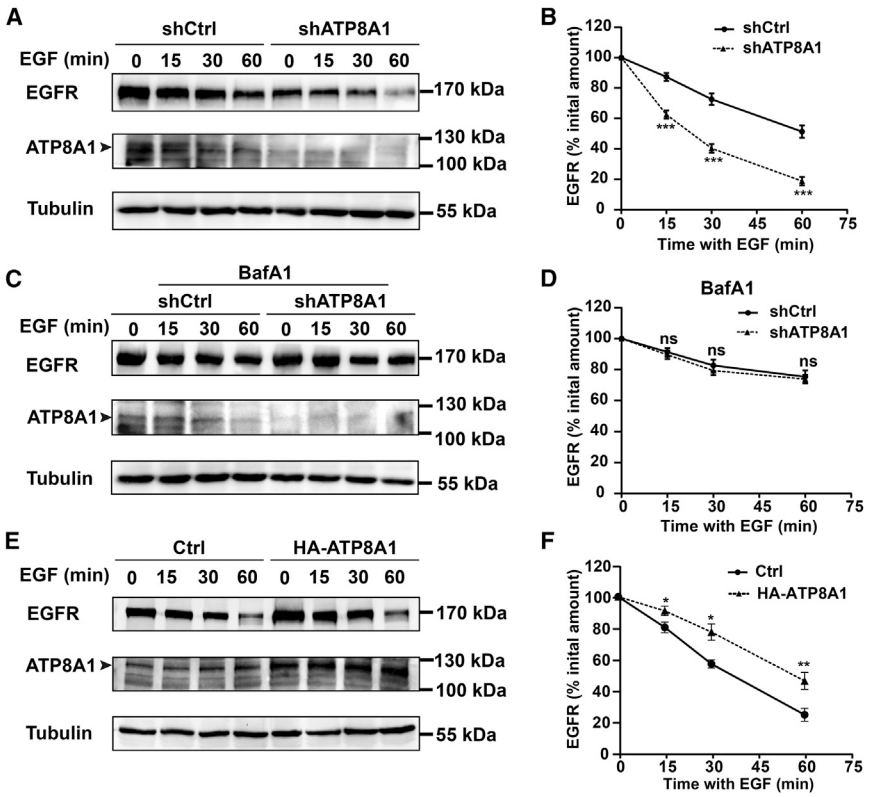

Figure 3. ATP8A1 negatively regulates EGF-induced EGFR degradation

(A and C) Control or shATP8A1 stable cell lines were starved in the absence (A) or presence (C) of 500 nM BafA1 for 12 h and stimulated with 100 ng/mL EGF for indicated time periods, followed by whole cell lysate harvest for immunoblotting analysis of EGFR levels.

(B and D) Quantification of the levels of EGFR from the analysis in A (B) or C (D). Data are displayed as mean ± SD, $N = 3$ from three independent experiments. ***$p < 0.001$; ns = non-significant by unpaired two-tailed Student's t test.

(E) Cells were transiently transfected with control or HA-ATP8A1, starved for 12 h and stimulated with 100 ng/mL EGF for indicated time periods, followed by whole cell lysate harvest for immunoblotting analysis of EGFR levels.

(F) Quantification of the levels of EGFR from the analysis in E. Data are displayed as mean ± SD, $N = 3$ from three independent experiments. *$p < 0.05$; **$p < 0.01$ by unpaired two-tailed Student's t test.

box indicates the central region of the endosome lumen. An analysis of 30 endosomes from multiple cells and experiments revealed a 6.76-fold increase of Alexa 555-EGF in the endosomal lumen in ATP8A1-depleted cells (Figure 5F). Re-expressing shRNA-resistant ATP8A1 but not E191Q, a mutant abolishing the catalytic ability of ATP8A1 flippase,[2] in shATP8A1 cells recovered the accelerated EGF transfer into MVBs (Figures 5D and S5). Collectively, these results indicated that depletion of ATP8A1 promotes EGF transfer through MVBs, which depends on its flippase catalytic activity. Moreover, transfer of EGF through the MVBs was not obviously changed in ATP11A-depleted cells (Figure S5), supporting that this arm of degradative transport is more sensitive to the endosomal but not PM-associated PS translocation.

We further examined the effect of ATP8A1 overexpression on EGF transfer through MVBs. Cells were co-expressed with EGFP-ATP8A1 and BFP-Rab5Q79L following Alexa 555-EGF pulse for indicated time. As seen in Figure 5G, upon 30 min of incubation, Alexa 555-EGF internalized and concentrated predominantly in ILVs of EGFP-ATP8A1 non-transfected cells (depicted by yellow arrow). In contrast, in neighboring EGFP-ATP8A1-expressing cells, Alexa 555-EGF was predominantly accumulated on the limiting membrane of the enlarged endosomes (depicted by white arrow). Alexa 555-EGF fluorescence in the endosomal lumen of ATP8A1-overexpressing cells was calculated to be reduced by 90.2% compared with control cells, in line with delayed transfer of EGF into the MVBs (Figures 5G and 5H). However, upon 60 min of incubation, the extent of Alexa 555-EGF moved into the ILVs of ATP8A1-overexpressing cells (depicted by white arrow) is similar to the ATP8A1-negative cells (depicted by yellow arrow) (Figures 5I and 5J). Together, these data supported that ATP8A1 negatively regulates EGF transit through MVBs.

To generalize our findings to other degradative cargos, we also assessed ATP8A1 regulation for muscarinic acetylcholine receptor (mAChR) M2, a GPCR member destined to lysosomes for degradation upon ligand-stimulation.[34,35] Carbacol (CCh) stimulation led to the surface-localized M2 receptor internalize and transit into Rab5Q79L-enlarged endosomes. Following exposure to CCh from 30 min to 90 min, the amount of MVBs containing internalized EGFP-M2 is significantly increased upon depletion of ATP8A1 (Figure S6). These results indicate that depletion of ATP8A1 affects certain lysosomal-destined cargos transit through MVBs.

ATP8A1-translocated endosomal PS fine-tunes the MVB formation

To decipher the mechanism underlying ATP8A1-regulated transport on degradative pathway, we next examined how the core machinery mediating sorting into the ILVs of MVBs is affected by ATP8A1 depletion. Endosomal sorting complex required for transport (ESCRT) molecules are central players in the endosomal sorting of EGFR and degradative cargoes destined to lysosomes.[29,32] HRS (hepatocyte growth factor-regulated Tyr-kinase substrate), component of ESCRT-0, localizes on early endosomes/sorting endosomes to recognize and capture ubiquitinated proteins for further degradation or sorting.[36,37] To visualize the ESCRT recruitment on MVBs, we examined the HRS foci on Rab5Q79L-enlarged endosomes in ATP8A1-depleting HeLa cells (Figure 6A). Quantification based on the line scan profiles showed that the HRS foci located along the contour of enlarged endosomes significantly increased by about 65.64%,

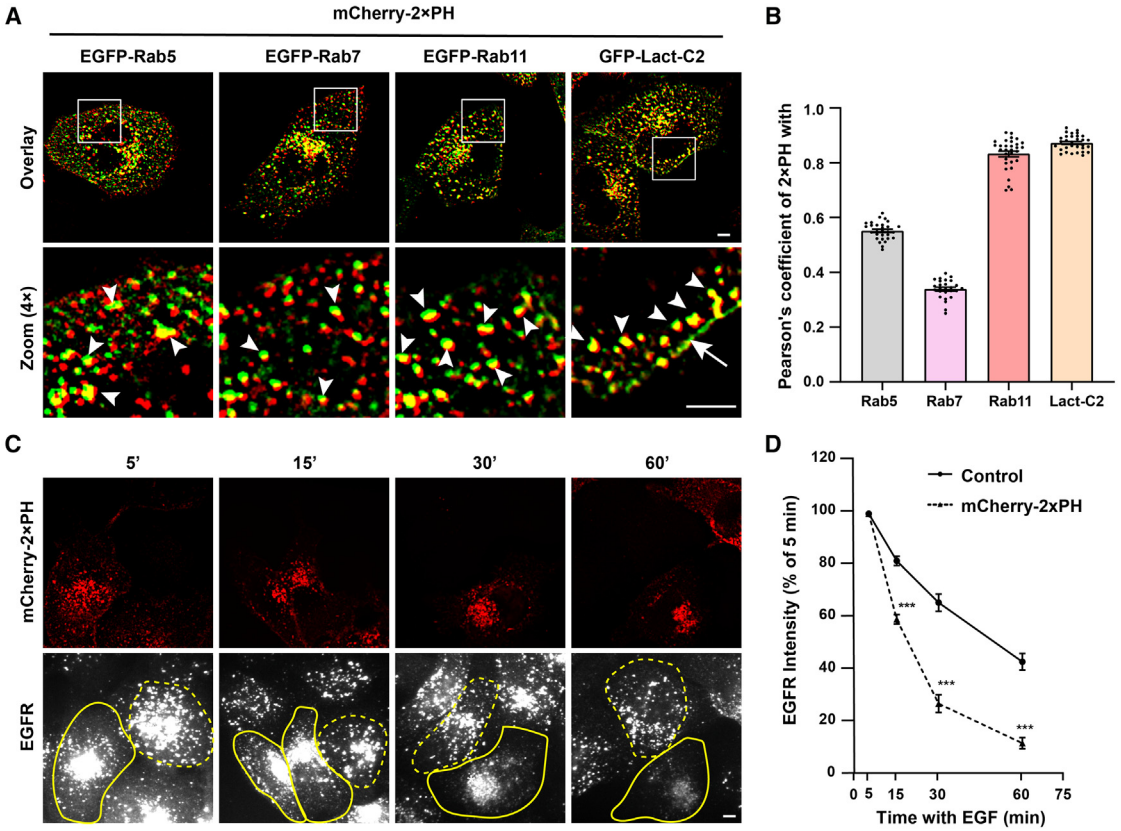

Figure 4. Blocking endosomal PS promotes EGF-induced EGFR degradation

(A) Confocal micrographs showing localization of mCherry-2×PH with respect to EGFP-tagged Rab5, Rab7, Rab11, and Lact-C2. The arrowheads in the magnified images mark the overlapped pixels. The arrow marks the PM. Scale bar, 5 μm.

(B) Quantification of the Pearson's correlation coefficient for the co-localization of mCherry-2×PH with different compartment markers from A. Data are displayed as mean ± SEM, $N \geq 25$ cells from three independent experiments.

(C) Overexpression of mCherry-2×PH accelerates EGF-induced EGFR degradation. mCherry-2×PH transfected HeLa cells were stimulated with 100 ng/mL EGF for indicated time periods followed by immunostaining with anti-EGFR antibody and fixed for confocal image. The solid or dashed line depicts mCherry-2×PH expressing-positive or -negative cells, respectively. Scale bar, 5 μm.

(D) Quantification of FI of the cytoplasmic EGFR for each condition indicated in C. ***$p < 0.001$ by unpaired two-tailed Student's t test. Data are displayed as mean ± SD, $N \geq 25$ cells from three independent experiments.

the contour length occupied by HRS foci increased from 35.65% in vehicle cells to 59.05% in shATP8A1 cells (Figures 6B and 6C). ESCRT-0 on endosomes in turn recruits clathrin and sequesters ubiquitylated cargo in clathrin-coated microdomains.[30,38] Consistent with what observed for HRS foci, clathrin clusters on the Rab5Q79L-enlarged endosomes also slightly increased from 48.34% in vehicle cells to 58.17% in shATP8A1 cells (Figures 6D–6F, assessed by the contour length occupied by clathrin clusters in 6E). Similar increase was also assessed for ESCRT-I complex subunit Tsg101 (Figures 6G and S6H). Combined, these data indicated that increasing ESCRT complex components are recruited onto the limiting membrane of MVBs in ATP8A1-depleted cells.

In addition, the PS content in the cytoplasmic face of Rab5Q79L-enlarged endosomes was specially examined using the mCherry-Lact-C2 probe (Figure 6I). The average FI was decreased from 3123.14 to 2805.3, mild but of significant difference, indicating that the cytoplasmic facial PS in the MVB′s limiting membrane is reduced by the ATP8A1 depletion (Figure 6J). Moreover, the signal of mCherry-Lact-C2 in the lumen was also slightly increased (Figure 6K). Because mCherry-Lact-C2 could only probe the cytoplasmic but not luminal facial PS in the limiting membranes, these intraluminal Lact-C2 signals topologically derive from the cytoplasmic facial PS in the limiting membrane and indicate that the ILVs budding from the limiting membranes are increased. We speculated that ATP8A1 depletion increased luminal facial PS content in the endosome's limiting membrane, which fine-tunes the ILVs initiation and consequently promotes ESCRT component recruitment on the limiting membrane of the enlarged endosomes.

DISCUSSION

In this study, we showed that ATP8A1, a PS flipping P4-ATPase, localizes along the endo-lysosomal sorting endosomes, where it mediates PS transbilayer translocation and fine-tunes the MVBs

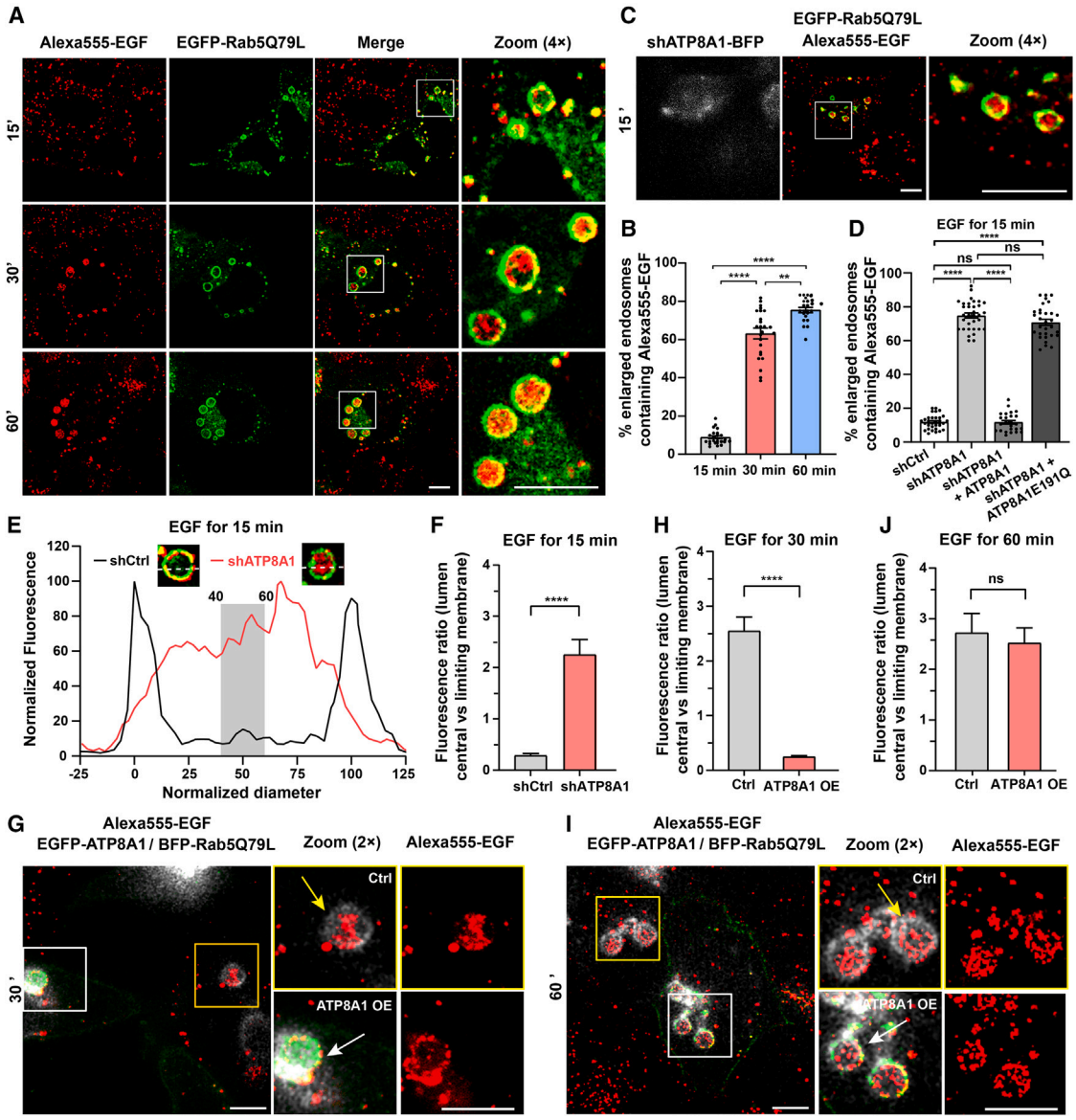

Figure 5. ATP8A1 tunes EGF transfer through ILVs of MVBs

(A) Confocal micrographs showing Alexa 555-EGF (100 ng/mL) internalized by the EGFP-Rab5Q79L-expressing cells for indicated time periods. Scale bar, 10 μm.

(B) Quantification of the Rab5Q79L-enlarged endosomes with Alexa 555-EGF in the lumen for the indicated conditions in A. $^{**}p < 0.01$; $^{****}p < 0.0001$ by Brown-Forsythe and Welch ANOVA with Dunnett T3 multiple comparison test at least 200 endosomes from $N \geq 25$ cells. Data are displayed as mean ± SEM from three independent experiments.

(C) ATP8A1-depletion accelerates EGF transfer in the ILVs of MVBs. shATP8A1-BFP-expressing cells were transfected with EGFP-Rab5Q79L and internalized Alexa 555-EGF for 15 min. Scale bar, 10 μm.

(D) Quantification of the Rab5Q79L-enlarged endosomes with Alexa 555-EGF in the lumen after 15 min uptake for control, shATP8A1, ATP8A1 WT or E191Q re-expressed shATP8A1 cells. $^{****}p < 0.0001$ by unpaired *t* test with Welch's correction, at least 200 endosomes from $N \geq 30$ cells. Data are displayed as mean ± SEM from three independent experiments.

(E) Representative line scan analysis showing the Alexa 555-EGF localization to the ILVs of endosomes in control or shATP8A1 cells upon 15 min uptake. The normalized diameter represents the diameter of the enlarged endosome, where 0 and 100 correspond to the pixel distances signifying the limiting membranes of the endosomes. The black and red traces represent the normalized fluorescence pixel intensity measured across the endosomes in control and ATP8A1-depleted cells, respectively, with the maximum pixel intensity across the line normalized to 100.

(F) The fluorescence ratio of luminal center to limiting membrane Alexa 555-EGF was calculated for control or shATP8A1 cells upon 15 min uptake of Alexa 555-EGF in E. The normalized fluorescence values of pixels from 40 to 60% of the normalized diameter were used to determine the mean central luminal fluorescence for each endosome. The values of pixels 0 and 100 were used to determine the mean limiting membrane fluorescence. $^{****}p < 0.0001$ by unpaired *t* test with Welch's correction, $N \geq 30$ endosomes. Data are displayed as mean ± SEM from three independent experiments.

(legend continued on next page)

formation, which ultimately affects the turnover kinetics of degradative cargo proteins. This is an attempt to explore how the manipulation of lipids other than PIPs plays a role in the functioning of endosomes.

Using cultured HeLa cells, we demonstrated that despite major localization in the cytosolic leaflet of PM, PS also localizes to the cytosolic leaflet of endosomal membranes, which is consistent with previous studies on various mammalian cells.[3,7] ATP8A1 is enriched in the endosomal compartments, especially in Rab7-positive LEs, but only in a fairly small proportion on PM (Figure 1). Depletion of ATP8A1 only visually decreased the endosomal-associated Lact-C2, but not that on the PM (Figures 2 and S2C–S2F). Moreover, by using Rab5Q79L to produce enlarged endosomes so as to magnify MVBs, slight but evident decrease in the Lact-C2 level was observed for the MVBs cytoplasmic face (Figure 6). In addition, EGF transfer through MVBs was speeded up and EGFR degradation in lysosomes was promoted in ATP8A1 depleting cells; in line with this, increasing luminal fluorescent Lact-C2 signal was observed in ATP8A1-depleting cells due to increased MVB formation (Figures 3, 5, and 6). By contrast, knockdown of either ATP11A or ATP11C, two other PS flippases, resulted in higher level of PS exposure on the exoplasmic leaflet of PM and had no remarkable impact on the transit of EGF through MVBs (Figures S2G, S2H, and S5). Collectively, these data indicated that at least in HeLa cells, ATP11A and/or ATP11C administer the PS asymmetry of PM, while ATP8A1 mainly plays a role for endosomal PS asymmetry, which affects the EGFR-laden MVB formation.

Previous studies demonstrated that the lipid components of EEs are similar to PM, but on maturation to LEs there is a decrease in sterols and PS and a dramatic increase in LBPA, which functions in MVBs generation.[39,40] In this work, we demonstrated that PS content is decreased from EE to LE cytosolic face, while the LEs harbor considerable amount of PS flippase ATP8A1 (Figures 1 and S2). Knockdown of ATP8A1, which presumably increases PS loading in the luminal leaflet of endosome's limiting membrane, promotes intraluminal membrane invagination and vesicle formation (Figure 6). This is the first study indicating PS role in the MVBs formation.

How P4-ATPases activity is harnessed to form a transport vesicle is an important cell biological and biophysical question. Previous studies indicated that P4-ATPases-induced changes in the transbilayer PS content can deform biological membranes that is essential to vesicle budding.[2,41] The yeast P4-ATPase Drs2 has been well characterized to induce positive curvature in the membrane (bending toward the cytosol) and, therefore, facilitate generation of tightly curved transport vesicles between TGN and EEs by translocating PS/PE.[11] TAT-5 deficiency in *C. elegans* causes substantial shedding of PM-derived extracellular vesicles, suggesting that TAT-5 flippase activity normally counterbalances a force on the PM that promotes outward bending (negative curvature).[42] In our study, ATP8A1 depletion promotes formation of ILVs, which is tightly associated with the flippase catalytic ability (Figures 6 and S5). In this regard, our results expand that physiologically PS flipping mediated by P4-ATPases fine-tunes membrane curvature and vesicle formation, not only for positive-curved vesicle budding toward the cytosol but also for negative-curved vesicle invagination toward the lumen.

Previous studies have revealed that PS is essential for recruitment of various vesicle formation proteins onto the late Golgi, RE or the PM, which further functions for positively curved membrane budding or fission in the cytosol.[2,3,15] In this study, shRNA-mediated knockdown of ATP8A1 compromises PS flipping to the cytosolic leaflets and concomitantly increases PS loading in the luminal leaflets of MVB's limiting membrane (Figure 6). The ILVs initiation, ESCRT component recruitment and ultimately the transfer of degradative cargos through MVBs were consequently modulated (Figures 5, 6, and S6). It is tempting to speculate that PS is multifaceted in recruiting vesicle formation proteins along the distinct post-endocytic pathways. On the recycling and retrograde pathway, the cytosolic leaflet-localized PS are required for the recruitment of proteins involved in membrane trafficking to cellular compartments; while on the late endosomal pathway, the subtle difference in the PS content between the luminal and cytosolic leaflet of endosomal limiting membrane possibly modulates the initiation of ILVs invagination.

Nevertheless, sporadic studies have implicated anionic lipid in initiating ESCRT activity at the membrane.[20,43] The link between PS-rich lipid domains and ESCRT-III activity was tested *in vitro* using giant unilamellar vesicle preparation.[21,44] It is tempting to characterize the ESCRT complex action and to examine *de novo* MVB formation affected by PS translocation *in vivo* in the future. We also wonder is there any machinery directly activated by PS in the endosomal cytosolic leaflet, which functions by opposing ESCRT-mediated ILV budding. Moreover, exosomes are known to be originated from MVBs fusion with the PM and release of ILVs. A novel exosome generated in Rab11-positive recycling endosomal MVBs has been reported recently.[45] Given tractable cargoes, it is intriguing to explore the possible impact of ATP8A1 manipulation on other type of MVBs in the future.

Together, our and other groups' studies suggested that at least in some cell types, ATP8A1 functions for flipping PS in the endosomal systems. We demonstrated that in HeLa cells ATP8A1 functions for PS asymmetry maintenance on the LEs, dysfunction of which will alter transport through MVBs. We also found AKT signaling is altered by ATP8A1 depletion. Considering the broad impact of ATP8A1 depletion on endosomal PS translocation, here we didn't determine the altered AKT signaling is caused by impaired recycling of EGFR from the EEs to the PM or accelerated transport through the MVBs or

(G and I) ATP8A1 overexpression retards but not blocks EGF transfer in the ILVs of MVBs. EGFP-ATP8A1-overexpressed cells were co-transfected with BFP-Rab5Q79L to enlarge endosomes and internalized Alexa 555-EGF (100 ng/mL) for 30 min (G) or 60 min (I). Yellow or white box depicts EGFP-ATP8A1-negative or -positive expressing cells and was zoomed in to the right, respectively. The arrows indicate the position of Alexa 555-EGF in the ATP8A1-negative (control) or -positive (ATP8A1-OE) cells. Scale bars, 10 μm.

(H and J) The fluorescence ratio of luminal center to limiting membrane Alexa 555-EGF was calculated for control or ATP8A1-OE cells upon 30 min (H) or 60 min (J) uptake of Alexa 555-EGF in G or I. ****$p < 0.0001$; ns = non-significant by unpaired t test with Welch's correction in (H) and unpaired two-tailed Student's t test in (J), $N \geq 30$ endosomes. Data are displayed as mean ± SEM.

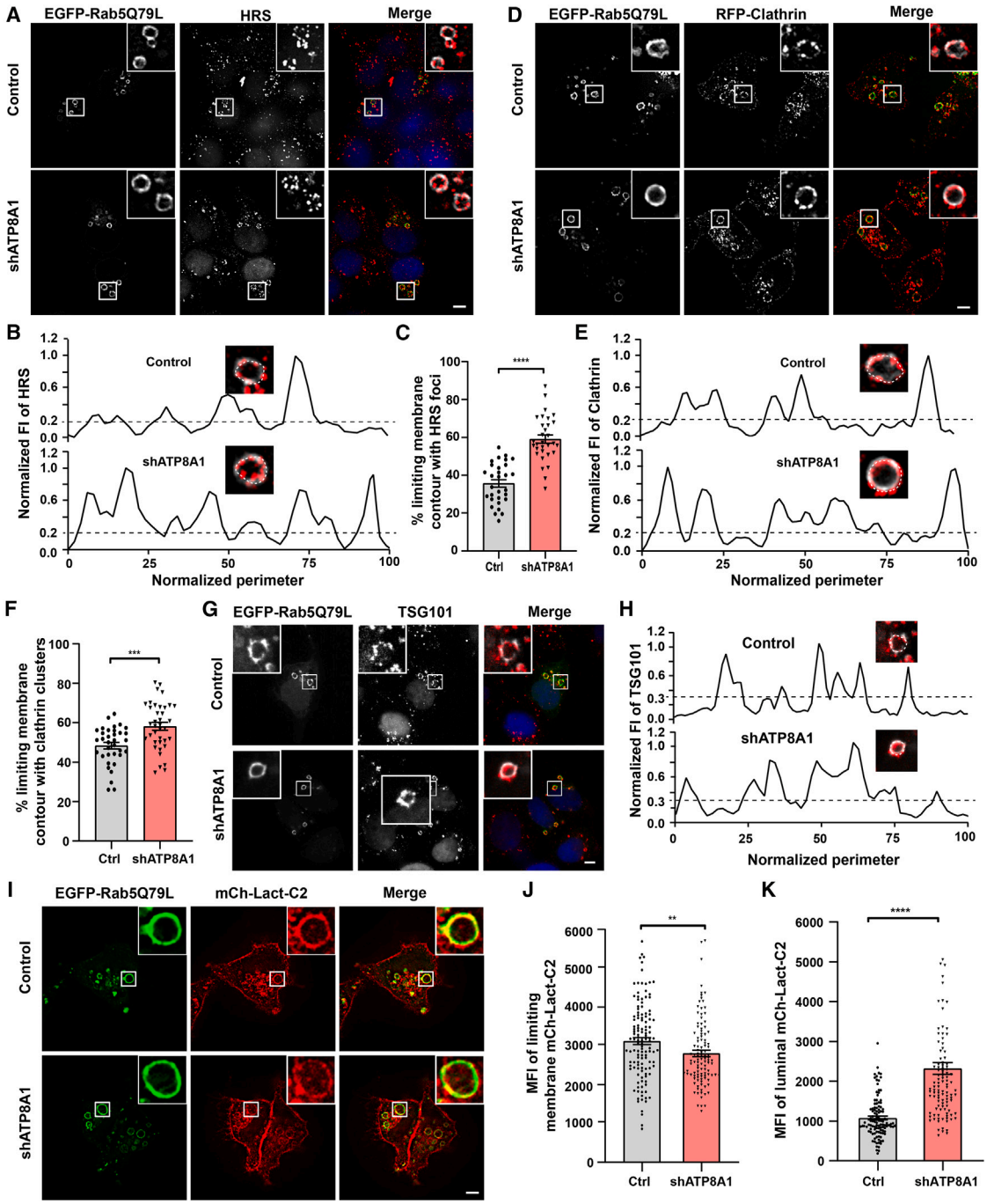

Figure 6. ATP8A1 depletion promotes ESCRT assembly on the MVBs

(A) Confocal micrographs showing the control or shATP8A1 cells that were transfected with EGFP-RabQ79L and immune-stained by anti-HRS antibody and DAPI. Insets show the HRS foci decorated on Rab5Q79L-enlarged endosomes. Scale bar, 10 μm.

(B) Line scan profiles of HRS foci along the contour of EGFP-Rab5Q79L-enlarged endosomes in A.

(C) The limiting membrane contour length decorated by HRS foci was calculated for enlarged endosomes in control or shATP8A1 cells. Pixels with normalized fluorescence values exceeding 0.2 (the dashed line denotes the threshold value) in B were counted as HRS-occupied limiting membrane length and summed, which was expressed as the percentage of the total limiting membrane length. ****$p < 0.0001$ by unpaired two-tailed Student's t test, $N \geq 30$ endosomes. Data are displayed as mean ± SEM from three independent experiments.

(D) Confocal micrographs showing the control or shATP8A1 cells that were co-transfected with EGFP-RabQ79L and RFP-Clathrin. Insets show the clathrin clusters decorated on Rab5Q79L-enlarged endosomes. Scale bar, 10 μm.

(E) Line profiles of clathrin clusters along the contour of EGFP-Rab5Q79L-enlarged endosomes in D.

(legend continued on next page)

both.[46] Nevertheless, together with the altered YAP signaling by ATP8A1 depletion,[4] this study points to impact of PS translocation on endosomal transport and associated spatial regulation of signaling, which deserve further investigation in the future.

We also noticed the discrepancy between this study and Lee et al.'s work, in which ATP8A1 knockdown did not affect the traffic of EGF to LAMP1-positive lysosomes in COS-1 cells.[2] It may be due to the different assay and cell types used in these two studies, since ATP8A1 appears not localize to organelles other than REs in COS-1 cells. So far, only ATP8A1 and ATP9A have been implicated in endosomal transport.[2,13,47] Exploring our knowledge on the P4-ATPases subcellular localization or their expression profiles in different tissues will help understanding how alternative P4-ATPases are involved in cellular processes like vesicular formation or protein sorting, etc.[10,15,42] An important goal in the future is to better define the extent to which different mechanisms contribute to membrane curvature for individual vesicle budding events and how different mechanisms are integrated and controlled. Moreover, is there any downstream effector that senses membrane curvature and/or negative charge imparted to the luminal leaflet of MVBs?

Limitations of the study

The membrane communication within cells is a multiple pathway-mediated dynamic and complex process. In this study, GFP-Lact-C2 detected PS in the cytoplasmic face of endosomal membranes is only slightly reduced in ATP8A1-depleted cells compared with vehicle cells, which is either due to the incomplete knockdown of ATP8A1 or due to compensation by the constant membrane flow from the PM through the endocytic route. Scramblases that mediate bidirectional transbilayer movement of phospholipids may also participate in the exposure of PS at the cytosolic leaflet in ATP8A1-depleted cells. It is still challenging to accurately identify and assess PS translocation on endosomes and coherently the involved physiological functions at the live-cell level. Moreover, whether ATP8A1 or other P4-ATPases locates and functions divergently in various cell types deserve further investigation in the future.

RESOURCE AVAILABILITY

Lead contact

Requests for further information and resources should be directed to and will be fulfilled by the lead contact, Rongying Zhang (ryzhang@hust.edu.cn).

Materials availability

All cell lines and plasmids used in this study are available to the scientific community. Please email the lead contact.

Data and code availability

- All date reported in this paper will be shared by the lead contact upon request.
- This paper does not report original code.
- Any additional information required to reanalyze the data reported will be shared by the lead contact upon request.

ACKNOWLEDGMENTS

We thank Dr. Emmanuel Boucrot (Institute of Structural and Molecular Biology, University College London, London, UK), Dr. James W. Wells (University of Toronto), Dr. Xinjun Zhang (Sichuan Provincial People's Hospital, University of Electronic Science and Technology of China, Chengdu, China), and Dr. Yuhui Zhang (Wuhan National Laboratory for Optoelectronics, Huazhong University of Science and Technology, Wuhan, China) for kindly donating material. This work was supported by the National Natural Science Foundation of China (32270739), and the Major Research Plan of the National Natural Science Foundation of China (91954107) to R.Z., and also by Hebei Natural Science Foundation of China (C2024402052) to Y.T.

AUTHOR CONTRIBUTIONS

Conceptualization, R.Z.; investigation, Z.L., Y.T., C.L., and Y.W.; methodology, Z.L., Y.T., C.L., and R.Z.; formal analysis, Z.L., Y.T., and C.L.; funding acquisition, R.Z. and Y.T.; project administration, R.Z.; original draft, R.Z.; writing and review and editing, R.Z., Z.L., P.Y., and Y.T.

DECLARATION OF INTERESTS

The authors declare no competing interests.

STAR★METHODS

Detailed methods are provided in the online version of this paper and include the following:

- KEY RESOURCES TABLE
- EXPERIMENTAL MODEL AND STUDY PARTICIPANT DETAILS
  - Cell lines
- METHOD DETAILS
  - Cell transfection
  - DNA constructs
  - Generation of lentiviral-based stable cell lines
  - Western blotting
  - Quantitative real-time polymerase chain reaction (qRT-PCR)
  - Flow cytometry
  - Immunofluorescence
  - Confocal microscopy
  - Cargo proteins internalization and trafficking assay
  - Imaging analysis
- QUANTIFICATION AND STATISTICAL ANALYSIS

(F) The limiting membrane contour length decorated by clathrin cluster was calculated for enlarged endosomes in control or shATP8A1 cells. ***$p < 0.001$ by unpaired two-tailed Student's t test, $N \geq 30$ endosomes. Data are displayed as mean ± SEM from three independent experiments.
(G) Confocal micrographs showing antibody-stained TSG101 distribution on the EGFP-Rab5Q79L-enlarged endosomes in control or shATP8A1 cells. Nuclei were stained with DAPI. Scale bar, 10 μm.
(H) Line scan profiles of TSG101 foci along the contour of EGFP-Rab5Q79L-enlarged endosomes in G.
(I–K) ATP8A1-depletion slightly reduced the PS content on the cytosolic leaflets of Rab5Q79L-enlarged endosomes. (I) Confocal micrographs showing the control or shATP8A1 cells that were co-transfected with EGFP-Rab5Q79L and mCherry-Lact-C2. Insets show the mCherry-Lact-C2 on the cytosolic leaflets of the Rab5Q79L-enlarged endosomes. Scale bar, 10 μm. (J) Quantification of the mean FI of the cytosolic leaflets-localized mCherry-Lact-C2 on the enlarged endosomes in G. **$p < 0.01$ by Mann-Whitney test, $N \geq 100$ endosomes. Data are displayed as mean ± SEM from three independent experiments. (K) Quantification of the mean FI of luminal mCherry-LactC2 in the enlarged endosomes in G. ****$p < 0.0001$ by Mann-Whitney test, $N \geq 100$ endosomes. Data are displayed as mean ± SEM from three independent experiments.

SUPPLEMENTAL INFORMATION

Supplemental information can be found online at https://doi.org/10.1016/j.isci.2025.111973.

Received: July 24, 2024
Revised: November 20, 2024
Accepted: February 5, 2025
Published: February 11, 2025

REFERENCES

1. Shin, H.-W., and Takatsu, H. (2020). Phosphatidylserine exposure in living cells. Crit. Rev. Biochem. Mol. Biol. *55*, 166–178. https://doi.org/10.1080/10409238.2020.1758624.
2. Lee, S., Uchida, Y., Wang, J., Matsudaira, T., Nakagawa, T., Kishimoto, T., Mukai, K., Inaba, T., Kobayashi, T., Molday, R.S., et al. (2015). Transport through recycling endosomes requires EHD1 recruitment by a phosphatidylserine translocase. EMBO J. *34*, 669–688. https://doi.org/10.15252/embj.201489703.
3. Hasegawa, J., Uchida, Y., Mukai, K., Lee, S., Matsudaira, T., and Taguchi, T. (2021). A Role of Phosphatidylserine in the Function of Recycling Endosomes. Front. Cell Dev. Biol. *9*, 783857. https://doi.org/10.3389/fcell.2021.783857.
4. Matsudaira, T., Mukai, K., Noguchi, T., Hasegawa, J., Hatta, T., Iemura, S.-I., Natsume, T., Miyamura, N., Nishina, H., Nakayama, J., et al. (2017). Endosomal phosphatidylserine is critical for the YAP signalling pathway in proliferating cells. Nat. Commun. *8*, 1246. https://doi.org/10.1038/s41467-017-01255-3.
5. Uchida, Y., Hasegawa, J., Chinnapen, D., Inoue, T., Okazaki, S., Kato, R., Wakatsuki, S., Misaki, R., Koike, M., Uchiyama, Y., et al. (2011). Intracellular phosphatidylserine is essential for retrograde membrane traffic through endosomes. Proc. Natl. Acad. Sci. USA *108*, 15846–15851. https://doi.org/10.1073/pnas.1109101108.
6. Inoue, C., Mukai, K., Matsudaira, T., Nakayama, J., Kono, N., Aoki, J., Arai, H., Uchida, Y., and Taguchi, T. (2023). PPP1R12A is a recycling endosomal phosphatase that facilitates YAP activation. Sci. Rep. *13*, 19740. https://doi.org/10.1038/s41598-023-47138-0.
7. Fairn, G.D., Schieber, N.L., Ariotti, N., Murphy, S., Kuerschner, L., Webb, R.I., Grinstein, S., and Parton, R.G. (2011). High-resolution mapping reveals topologically distinct cellular pools of phosphatidylserine. J. Cell. Biol. *194*, 257–275. https://doi.org/10.1083/jcb.201012028.
8. Yeung, T., Gilbert, G.E., Shi, J., Silvius, J., Kapus, A., and Grinstein, S. (2008). Membrane phosphatidylserine regulates surface charge and protein localization. Science *319*, 210–213. https://doi.org/10.1126/science.1152066.
9. Hirama, T., Lu, S.M., Kay, J.G., Maekawa, M., Kozlov, M.M., Grinstein, S., and Fairn, G.D. (2017). Membrane curvature induced by proximity of anionic phospholipids can initiate endocytosis. Nat. Commun. *8*, 1393. https://doi.org/10.1038/s41467-017-01554-9.
10. van der Mark, V.A., Elferink, R.P.J.O., and Paulusma, C.C. (2013). P4 ATPases: Flippases in Health and Disease. Int. J. Mol. Sci. *14*, 7897–7922. https://doi.org/10.3390/ijms14047897.
11. Xu, P., Baldridge, R.D., Chi, R.J., Burd, C.G., and Graham, T.R. (2013). Phosphatidylserine flipping enhances membrane curvature and negative charge required for vesicular transport. J. Cell Biol. *202*, 875–886. https://doi.org/10.1083/jcb.201305094.
12. Best, J.T., Xu, P., and Graham, T.R. (2019). Phospholipid flippases in membrane remodeling and transport carrier biogenesis. Curr. Opin. Cell Biol. *59*, 8–15. https://doi.org/10.1016/j.ceb.2019.02.004.
13. Meng, T., Chen, X., He, Z., Huang, H., Lin, S., Liu, K., Bai, G., Liu, H., Xu, M., Zhuang, H., et al. (2023). ATP9A deficiency causes ADHD and aberrant endosomal recycling via modulating RAB5 and RAB11 activity. Mol. Psychiatry. *28*, 1219–1231. https://doi.org/10.1038/s41380-022-01940-w.
14. Miyata, Y., Yamada, K., Nagata, S., and Segawa, K. (2022). Two types of type IV P-type ATPases independently re-establish the asymmetrical distribution of phosphatidylserine in plasma membranes. J. Biol. Chem. *298*, 102527. https://doi.org/10.1016/j.jbc.2022.102527.
15. Shin, H.-W., and Takatsu, H. (2019). Substrates of P4-ATPases: beyond aminophospholipids (phosphatidylserine and phosphatidylethanolamine). FASEB. J. *33*, 3087–3096. https://doi.org/10.1096/fj.201801873R.
16. Bryde, S., Hennrich, H., Verhulst, P.M., Devaux, P.F., Lenoir, G., and Holthuis, J.C.M. (2010). CDC50 Proteins Are Critical Components of the Human Class-1 P4-ATPase Transport Machinery. J. Biol. Chem. *285*, 40562–40572. https://doi.org/10.1074/jbc.M110.139543.
17. Takatsu, H., Baba, K., Shima, T., Umino, H., Kato, U., Umeda, M., Nakayama, K., and Shin, H.-W. (2011). ATP9B, a P4-ATPase (a Putative Aminophospholipid Translocase), Localizes to the trans-Golgi Network in a CDC50 Protein-independent Manner. J. Biol. Chem. *286*, 38159–38167. https://doi.org/10.1074/jbc.M111.281006.
18. Kato, U., Inadome, H., Yamamoto, M., Emoto, K., Kobayashi, T., and Umeda, M. (2013). Role for Phospholipid Flippase Complex of ATP8A1 and CDC50A Proteins in Cell Migration. J. Biol. Chem. *288*, 4922–4934. https://doi.org/10.1074/jbc.M112.402701.
19. Kook, S., Wang, P., Meng, S., Jetter, C.S., Sucre, J.M.S., Benjamin, J.T., Gokey, J.J., Hanby, H.A., Jaume, A., Goetzl, L., et al. (2021). AP-3-dependent targeting of flippase ATP8A1 to lamellar bodies suppresses activation of YAP in alveolar epithelial type 2 cells. Proc. Natl. Acad. Sci. USA *118*, e2025208118. https://doi.org/10.1073/pnas.2025208118.
20. Gruenberg, J. (2020). Life in the lumen: The multivesicular endosome. Traffic *21*, 76–93. https://doi.org/10.1111/tra.12715.
21. Booth, A., Marklew, C.J., Ciani, B., and Beales, P.A. (2021). The influence of phosphatidylserine localisation and lipid phase on membrane remodelling by the ESCRT-II/ESCRT-III complex. Faraday. Discuss. *232*, 188–202. https://doi.org/10.1039/d0fd00042f.
22. Wang, J., Molday, L.L., Hii, T., Coleman, J.A., Wen, T., Andersen, J.P., and Molday, R.S. (2018). Proteomic Analysis and Functional Characterization of P4-ATPase Phospholipid Flippases from Murine Tissues. Sci. Rep. *8*, 10795. https://doi.org/10.1038/s41598-018-29108-z.
23. Liou, A.Y., Molday, L.L., Wang, J., Andersen, J.P., and Molday, R.S. (2019). Identification and functional analyses of disease-associated P4-ATPase phospholipid flippase variants in red blood cells. J. Biol. Chem. *294*, 6809–6821. https://doi.org/10.1074/jbc.RA118.007270.
24. Yang, Y., Sun, K., Liu, W., Li, X., Tian, W., Shuai, P., and Zhu, X. (2021). The phosphatidylserine flippase β-subunit Tmem30a is essential for normal insulin maturation and secretion. Mol. Ther. *29*, 2854–2872. https://doi.org/10.1016/j.ymthe.2021.04.026.
25. Levano, K., Punia, V., Raghunath, M., Debata, P.R., Curcio, G.M., Mogha, A., Purkayastha, S., McCloskey, D., Fata, J., and Banerjee, P. (2012). Atp8a1 deficiency is associated with phosphatidylserine externalization in hippocampus and delayed hippocampus-dependent learning. J. Neurochem. *120*, 302–313. https://doi.org/10.1111/j.1471-4159.2011.07543.x.
26. Mayle, K.M., Le, A.M., and Kamei, D.T. (2012). The intracellular trafficking pathway of transferrin. Biochim. Biophys. Acta. *1820*, 264–281. https://doi.org/10.1016/j.bbagen.2011.09.009.
27. Takatsu, H., Tanaka, G., Segawa, K., Suzuki, J., Nagata, S., Nakayama, K., and Shin, H.-W. (2014). Phospholipid Flippase Activities and Substrate Specificities of Human Type IV P-type ATPases Localized to the Plasma Membrane. J. Biol. Chem. *289*, 33543–33556. https://doi.org/10.1074/jbc.M114.593012.
28. Platre, M.P., Noack, L.C., Doumane, M., Bayle, V., Simon, M.L.A., Maneta-Peyret, L., Fouillen, L., Stanislas, T., Armengot, L., Pejchar, P., et al. (2018). A Combinatorial Lipid Code Shapes the Electrostatic Landscape of Plant Endomembranes. Dev. Cell. *45*, 465–480.e11. https://doi.org/10.1016/j.devcel.2018.04.011.

29. Sorkin, A., and Goh, L.K. (2009). Endocytosis and intracellular trafficking of ErbBs. Exp. Cell Res. *315*, 683–696. https://doi.org/10.1016/j.yexcr.2008.07.029.

30. Raiborg, C., Bache, K.G., Gillooly, D.J., Madshus, I.H., Stang, E., and Stenmark, H. (2002). Hrs sorts ubiquitinated proteins into clathrin-coated microdomains of early endosomes. Nat. Cell. Biol. *4*, 394–398. https://doi.org/10.1038/ncb791.

31. Wegener, C.S., Malerød, L., Pedersen, N.M., Prodiga, C., Bakke, O., Stenmark, H., and Brech, A. (2009). Ultrastructural characterization of giant endosomes induced by GTPase-deficient Rab5. Histochem. Cell. Biol. *133*, 41–55. https://doi.org/10.1007/s00418-009-0643-8.

32. Hanafusa, H., Ishikawa, K., Kedashiro, S., Saigo, T., Iemura, S.-I., Natsume, T., Komada, M., Shibuya, H., Nara, A., and Matsumoto, K. (2011). Leucine-rich repeat kinase LRRK1 regulates endosomal trafficking of the EGF receptor. Nat. Commun. *2*, 158. https://doi.org/10.1038/ncomms1161.

33. Rosciglione, S., Thériault, C., Boily, M.-O., Paquette, M., and Lavoie, C. (2014). Gαs regulates the post-endocytic sorting of G protein-coupled receptors. Nat. Commun. *5*, 4556. https://doi.org/10.1038/ncomms5556.

34. Wan, M., Zhang, W., Tian, Y., Xu, C., Xu, T., Liu, J., and Zhang, R. (2015). Unraveling a molecular determinant for clathrin-independent internalization of the M2 muscarinic acetylcholine receptor. Sci. Rep. *5*, 11408. https://doi.org/10.1038/srep11408.

35. Zenko, D., Thompson, D., and Hislop, J.N. (2020). Endocytic sorting and downregulation of the M2 acetylcholine receptor is regulated by ubiquitin and the ESCRT complex. Neuropharmacology *162*, 107828. https://doi.org/10.1016/j.neuropharm.2019.107828.

36. Marchese, A., Raiborg, C., Santini, F., Keen, J.H., Stenmark, H., and Benovic, J.L. (2003). The E3 ubiquitin ligase AIP4 mediates ubiquitination and sorting of the G protein-coupled receptor CXCR4. Dev. Cell *5*, 709–722. https://doi.org/10.1016/s1534-5807(03)00321-6.

37. Hislop, J.N., Marley, A., and von Zastrow, M. (2004). Role of Mammalian Vacuolar Protein-sorting Proteins in Endocytic Trafficking of a Non-ubiquitinated G Protein-coupled Receptor to Lysosomes. J. Biol. Chem. *279*, 22522–22531. https://doi.org/10.1074/jbc.M311062200.

38. Raiborg, C., and Stenmark, H. (2009). The ESCRT machinery in endosomal sorting of ubiquitylated membrane proteins. Nature *458*, 445–452. https://doi.org/10.1038/nature07961.

39. van Meer, G., Voelker, D.R., and Feigenson, G.W. (2008). Membrane lipids: where they are and how they behave. Nat. Rev. Mol. Cell. Biol. *9*, 112–124. https://doi.org/10.1038/nrm2330.

40. Matsuo, H., Chevallier, J., Mayran, N., Le Blanc, I., Ferguson, C., Faure, J., Blanc, N.S., Matile, S., Dubochet, J., Sadoul, R., et al. (2004). Role of LBPA and Alix in multivesicular liposome formation and endosome organization. Science *303*, 531–534. https://doi.org/10.1126/science.1092425.

41. Graham, T.R., and Kozlov, M.M. (2010). Interplay of proteins and lipids in generating membrane curvature. Curr. Opin. Cell. Biol. *22*, 430–436. https://doi.org/10.1016/j.ceb.2010.05.002.

42. Beer, K.B., Rivas-Castillo, J., Kuhn, K., Fazeli, G., Karmann, B., Nance, J.F., Stigloher, C., and Wehman, A.M. (2018). Extracellular vesicle budding is inhibited by redundant regulators of TAT-5 flippase localization and phospholipid asymmetry. Proc. Natl. Acad. Sci. USA *115*, E1127–E1136. https://doi.org/10.1073/pnas.1714085115.

43. Lee, I.H., Kai, H., Carlson, L.A., Groves, J.T., and Hurley, J.H. (2015). Negative membrane curvature catalyzes nucleation of endosomal sorting complex required for transport (ESCRT)-III assembly. Proc. Natl. Acad. Sci. USA *112*, 15892–15897. https://doi.org/10.1073/pnas.1518765113.

44. Avalos-Padilla, Y., Knorr, R.L., Javier-Reyna, R., García-Rivera, G., Lipowsky, R., Dimova, R., and Orozco, E. (2018). The Conserved ESCRT-III Machinery Participates in the Phagocytosis of Entamoeba histolytica. Front. Cell. Infect. Microbiol. *8*, 53. https://doi.org/10.3389/fcimb.2018.00053.

45. Fan, S.J., Kroeger, B., Marie, P.P., Bridges, E.M., Mason, J.D., McCormick, K., Zois, C.E., Sheldon, H., Khalid Alham, N., Johnson, E., et al. (2020). Glutamine deprivation alters the origin and function of cancer cell exosomes. EMBO. J. *39*, e103009. https://doi.org/10.15252/embj.2019103009.

46. Nishimura, Y., Takiguchi, S., Ito, S., and Itoh, K. (2015). EGF-stimulated AKT activation is mediated by EGFR recycling via an early endocytic pathway in a gefitinib-resistant human lung cancer cell line. Int. J. Oncol. *46*, 1721–1729. https://doi.org/10.3892/ijo.2015.2871.

47. Tanaka, Y., Ono, N., Shima, T., Tanaka, G., Katoh, Y., Nakayama, K., Takatsu, H., Shin, H.-W., and Nakano, A. (2016). The phospholipid flippase ATP9A is required for the recycling pathway from the endosomes to the plasma membrane. Mol. Biol. Cell. *27*, 3883–3893. https://doi.org/10.1091/mbc.E16-08-0586.

48. Pisterzi, L.F., Jansma, D.B., Georgiou, J., Woodside, M.J., Chou, J.T.C., Angers, S., Raicu, V., and Wells, J.W. (2010). Oligomeric size of the m2 muscarinic receptor in live cells as determined by quantitative fluorescence resonance energy transfer. J. Biol. Chem. *285*, 16723–16738. https://doi.org/10.1074/jbc.M109.069443.

49. Honsho, M., Abe, Y., and Fujiki, Y. (2017). Plasmalogen biosynthesis is spatiotemporally regulated by sensing plasmalogens in the inner leaflet of plasma membranes. Sci. Rep. *7*, 43936. https://doi.org/10.1038/srep43936.

50. He, W., Gea-Mallorquí, E., Colin-York, H., Fritzsche, M., Gillespie, G.M., Brackenridge, S., Borrow, P., and McMichael, A.J. (2023). Intracellular trafficking of HLA-E and its regulation. J. Exp. Med. *220*, e20221941. https://doi.org/10.1084/jem.20221941.

51. Bolte, S., and Cordelières, F.P. (2006). A guided tour into subcellular colocalization analysis in light microscopy. J. Microsc. *224*, 213–232. https://doi.org/10.1111/j.1365-2818.2006.01706.x.

52. Li, X., Létourneau, D., Holleran, B., Leduc, R., Lavigne, P., and Lavoie, C. (2017). Gαs protein binds ubiquitin to regulate epidermal growth factor receptor endosomal sorting. Proc. Natl. Acad. Sci. USA *114*, 13477–13482. https://doi.org/10.1073/pnas.1708215114.

STAR★METHODS

KEY RESOURCES TABLE

REAGENT or RESOURCE	SOURCE	IDENTIFIER
Antibodies		
rabbit polyclonal anti-ATP8A1	Proteintech	Cat# 21565-AP; RRID: AB_10734587
mouse monoclonal anti-EGFR	Proteintech	Cat# 18986-1-AP; RRID: AB_10596476
mouse monoclonal anti-HRS	Proteintech	Cat# 67818-1-Ig; RRID: AB_2918581
mouse monoclonal anti-TSG101	Santa Cruz Biotechnology	Cat# sc-7964; RRID: AB_671392
mouse monoclonal anti-Tubulin	Proteintech	Cat# 66031-1-Ig; RRID: AB_11042766
mouse monoclonal anti-LAMP1	The Developmental Studies Hybridoma Bank	Cat# H4A3; RRID: AB_2296838
mouse monoclonal anti-GAPDH	Proteintech	Cat# 60004-1-Ig; RRID: AB_2107436
rabbit monoclonal anti-Flag/DYKDDDDK tag	Proteintech	Cat# 20543-1-AP; RRID: AB_11232216
rabbit polyclonal anti-AKT	Cell Signaling Technology	Cat# 9272; RRID: AB_329827
rabbit monoclonal anti-Phospho-Akt (Ser473)	Cell Signaling Technology	Cat# 4058; RRID: AB_331168
rabbit polyclonal anti-Erk1/2	Cell Signaling Technology	Cat# 9102; RRID: AB_330744
rabbit polyclonal anti- phosphorylated Erk1/2	Cell Signaling Technology	Cat# 9101; RRID: AB_331646
goat anti-mouse polyclonal HRP IgG	Biosharp	Cat# BL001A; RRID: AB_2827665
goat anti-rabbit polyclonal HRP IgG	Biosharp	Cat# BL003A; RRID: AB_2827666
rabbit Alexa Fluor 488	Beyotime	Cat# A0428; RRID: AB_2893435
mouse Alexa Fluor 488	Jackson	Cat# 715-545-150; RRID: AB_2340846
mouse Alexa Fluor 555	Innovative Research	Cat# A21137; RRID: AB_1500824
mouse Cy3	Jackson	Cat# 715-165-150; RRID: AB_2340813
Chemicals, peptides, and recombinant proteins		
Dulbecco Modified Eagle's Medium	Thermo Fisher Scientific-Gibco	Cat# C11995500BT
Fetal bovine serum	Yeasen	Cat# 40130ES76
Opti-MEM™ I	Thermo Fisher Scientific-Gibco	Cat# 11058021
Penicillin-Streptomycin	HyClone	Cat# SV30010
Trypsin	Biosharp	Cat# BS130
Minimum Essential Medium (MEM) α	Thermo Fisher Scientific-Gibco	Cat# 41061029
Protease inhibitor cocktail tablets	Roche Diagnostics	Cat# 4693116001
EGF	Thermo Fisher Scientific-Gibco	Cat# PHG3011
Alexa Fluor® 555 EGF	Invitrogen™	Cat# E35350
TRITC-WGA	EY laboratories	Cat# R-2101-5
Cycloheximide	Aladdin	Cat# 66-81-9
DAPI	Sigma-Aldrich	Cat# D9542
Saponin	Sigma-Aldrich	Cat# S7900-25G
Paraformaldehyde	Sigma-Aldrich	Cat# 158127
Puromycin	Thermo Fisher Scientific-Gibco	Cat# A1113803
LysoTracker Deep Red	Invitrogen™	Cat# L12492
Carbachol	Sigma-Aldrich	Cat# 51-83-2
Critical commercial assays		
Lipofectamine™ 2000 Transfection Reagent	Invitrogen™	Cat# 11668019
Annexin V-FITC/PI Apoptosis detection Kit	Meilunbio	Cat# MA0428
Fixation/Permeabilization Kit	Becton, Dickinson and Company	Cat# 554714
ECL Western Blotting reagents	Thermo Fisher Scientific	Cat# 34094
Reverse Transcription Kit	Biosharp Life Science	Cat# BL696A

(*Continued on next page*)

Continued

REAGENT or RESOURCE	SOURCE	IDENTIFIER
Taq Pro Universal SYBR qPCR Master Mix	Vazyme	Cat# Q712
RNA-easy Isolation Reagent	Vazyme	Cat# R701
Mycolor One-Step Mycoplasma Detector	Vazyme	Cat# D201
Experimental models: Cell lines		
HeLa	This study	N/A
COS-7	This study	N/A
HEK293T	This study	N/A
HeLa-shATP8A1	This study	N/A
HeLa-shATP11A	This study	N/A
HeLa-ATP8A1-Flag	This study	N/A
Oligonucleotides		
EGFP-ATP8A1-F 5'-GTGAGGTACCGCGGGCCCGGGA TCCACCGGATC TAGATAAC-3'	This study	N/A
EGFP-ATP8A1-R 5'-GGATCCCGGGCCCGCGGTACCTC ACCATTCGTC GGGCCTCTGTTTC-3'	This study	N/A
mCherry-ATP8A1D409N-F 5'-TTAGCTTTGTCATGCAAAGCTGTCATTTGC-3'	This study	N/A
mCherry-ATP8A1D409N-R 5'-GCATGACAAAGCTAAGTCCAGGAA ATACTGTCG TAC-3'	This study	N/A
EGFP-ATP8A1-shRNA-resistant-F 5'-ACTATGAACCCACAGACACTG CTGCCATGGCGCG GACGTCCAATCTGAATGAGGAAC-3'	This study	N/A
EGFP-ATP8A1-shRNA-resistant-R 5'-GGCCAAGTTCCTCATTCAGATTGG ACGTCCGCGCCATGGCAGCAGTGTC TGTGGGTTC-3'	This study	N/A
BFP-ATP8A1-shRNA-resistant-F 5'-AACCGTCAGATCCGCTAGCGCTACCGGTCG CCACCATGAGTGAGCTGATTAAGGAGAAC-3'	This study	N/A
BFP–ATP8A1-shRNA-resistant-R 5'-GAATTCGAAGCTTGAGCTCGAGATCTGAGTCCGG AAAACTTGTGCCCCAATTTGCTAGG-3'	This study	N/A
BFP-ATP8A1E191Q- shRNA-resistant-F 5'-ACATCCAACTTAGATGGTCAAACAAACTTGAAAAT TAGACAGGGCTTACCAGC-3'	This study	N/A
BFP-ATP8A1E191Q- shRNA-resistant-R 5'-GCCCTGTCTAATTTTCAAGTTTGTTTGACCATCTA AGTTGGATG-3'	This study	N/A
HA-ATP8A1-F 5'-CTACGACGTGCCCGACTACGCCCCCACCATGCG GAGGACC-3'	This study	N/A
HA-ATP8A1-R 5'-ATCTCGAGGCCACCATGTACCCCTACGACGTGCC CGAC-3'	This study	N/A
mCherry-Rab7-F 5'-ACGGTACCAGCCACCATGACCTCTAGGAAGAAAG-3'	This study	N/A

(*Continued on next page*)

Continued

REAGENT or RESOURCE	SOURCE	IDENTIFIER
mCherry-Rab7-R 5'-GTTATCTAGATCTCAGCAACTGCAGCTTTC-3'	This study	N/A
mCherry-Rab11-F 5'-TCAGATCTCGAGATGGGCACCCGCGACGACGC-3'	This study	N/A
mCherry-Rab11-R 5'-GAATTCGAAGCTTTTATATGTTCTGACAGCACTGC-3'	This study	N/A
BFP-Rab5Q79L-F 5'-GGTCAAGAACGATACCATAGCCTAGCACCAATGT AC-3'	This study	N/A
BFP-Rab5Q79L-R 5'-ATGGTATCGTTCTTGACCAGCTGTATCCCATATTT C-3'	This study	N/A
mCherry-Lact-C2-F 5'-ATCTCGAGTGCACTGAACCCCTAGGCCTGAAG-3'	This study	N/A
mCherry-Lact-C2-R 5'-GAAGCTTCTAACAGCCCAGCAGCTCCACTCG-3'	This study	N/A
pLVX-puro-ATP8A1-Flag-F 5'-TACCGGACTCAGATCTCGAGATGCCCACCATGCG GAGGAC-3'	This study	N/A
pLVX-puro-ATP8A1-Flag-R 5'-CCTCCCCTACCCGGTAGAATTATCTAGATCACCA TTCGTCGGGCCTCTGTTTC-3'	This study	N/A
ATP8A1-F(qRT-PCR) 5'-GGCCTGCAGGCAGCTAATTCC-3'	This study	N/A
ATP8A1-R(qRT-PCR) 5'-GTGTTGAAGTCCAGGGCATTC-3'	This study	N/A
ATP11A-F(qRT-PCR) 5'-GACCCTGTAGTGAGGCCTTT-3'	This study	N/A
ATP11A-R(qRT-PCR) 5'-ACTCTGCCACACGTACTTCA-3'	This study	N/A
ATP811C-F(qRT-PCR) 5'-GGAACGTAATGCAATGGATGGG-3'	This study	N/A
ATP811C-R(qRT-PCR) 5'-GGTTAGTTCTAAGAGCTCAGTG-3'	This study	N/A
CDC50A-F(qRT-PCR) 5'-GAAAAAGAAAGGTATTGCTTGGTG-3'	This study	N/A
CDC50A-R(qRT-PCR) 5'-GTAATGTCAGCTGTATTACTACTG-3'	This study	N/A
GAPDH-F(qRT-PCR) 5'-CTCTGCTCCTCCTGTTCGAC-3'	This study	N/A
GAPDH-R(qRT-PCR) 5'-GCGCCCAATACGACCAAATC-3'	This study	N/A
Recombinant DNA		
shATP8A1-GFP shRNA sequence -GCTATGGCTCGAACATCTA	This study	N/A
shCDC50A-GFP shRNA sequence - GAGCTATTGCCAACAGCAT	This study	N/A
pLKO.1-puro-shATP8A1 shRNA sequence -GCTATGGCTCGAACATCTA	This study	N/A
pLKO.1-puro-shATP11A shRNA sequence -GCTGCTGTTCTACGTTGTCTT	This study	N/A
pLKO.1-puro-shATP11C shRNA sequence -GCTGTCGGATGGCACCATTAC	This study	N/A
GFP-Lact-C2	Addgene	Cat# 22852

(*Continued on next page*)

Continued

REAGENT or RESOURCE	SOURCE	IDENTIFIER
RFP-HRS	Addgene	Cat# 29685
ER-mCherry	Dr. Yuhui Zhang's lab	N/A
mCherry-Rab5	Dr. Emmanuel Boucrot's lab	N/A
pLVX-puro	Dr. Xinjun Zhang's lab	N/A
pLKO.1-puro	Dr. Xinjun Zhang's lab	N/A
psPAX2	Dr. Xinjun Zhang's lab	N/A
pMD2.G	Dr. Xinjun Zhang's lab	N/A
RFP-Clathrin	This study	N/A
TfR-EGFP	This study	N/A
CDC50A-Flag	This study	N/A
Golgi-mkate2	This study	N/A
EGFP-Rab5Q79L	This study	N/A
mCherry-2×PH	This study	N/A
Software and algorithms		
Fiji (ImageJ)	National Institutes of Health	https://imagej.nih.gov/ij/
AutoQuant×2	Media Cybernetics	N/A
QuantStudio 6 and 7 Flex	Applied Biosystems	N/A
FlowJo v10.0	Tree Star Inc	https://www.flowjo.com/solutions/flowjo
GraphPad Prism v8.0	GraphPad Prism Software	https://www.graphpad.com/

EXPERIMENTAL MODEL AND STUDY PARTICIPANT DETAILS

Cell lines

HeLa, Human Embryonic Kidney 293T (HEK 293T) and COS-7 cells were maintained in DMEM medium, supplemented with 10% (v/v) fetal bovine serum, 2mM L-glutamine, 100 U/ml penicillin and 100 U/ml streptomycin at 37°C in a 5% CO_2 humidified incubator. The cell lines have not been authenticated. Cells were free from mycoplasma infection. Sample size calculation was not conducted in this study.

METHOD DETAILS

Cell transfection

Cells were transfected with the indicated plasmid using lipofectamine 2000 according to the manufacturer's protocol (Thermo Fisher Scientific, UK) and used for experiments 24 h later. While for shRNAs (alone or in combination with plasmids) cells were processed 72 h after transfection.

DNA constructs

EGFP-tagged Rab5, Rab7 and Rab11 were gifts from Dr. Emmanuel Boucrot's lab. The plasmid ss-EGFP-M2 (ss, signal sequence) was a kind gift from James W. Wells's lab.[48] Lentiviral vector (pLVX-puro and pLKO.1-puro) and lentiviral packaging plasmids (psPAX2 and pMD2.G) were gifts from Dr. Xinjun Zhang's lab. ER-mCherry was gift from Dr. Yuhui Zhang's lab. GFP-Lact-C2 (Addgene, 22852) and RFP-HRS (Addgene, 29685) were purchased from Addgene. Unless stated otherwise, all EGFP-, mCherry-, RFP- and Flag-tagged plasmids were constructed by subcloning individual cDNA into the pEGFP-C1, pmCherry-C3, pcDNA3.1 and Pcmv-Tag4A-Flag backbone at specific restriction enzyme digestion sites. EGFP-ATP8A1D409N and EGFP-Rab5Q79L were cloned from the WT plasmids by base mutation. To construct the shATP8A1-GFP and shCDC50A-GFP plasmids, the nucleotide target sequence of the human ATP8A1 gene (5'-GCTATGGCTCGAACATCTA-3')[2] and CDC50A gene (5'-GAGCTATTGCCAACAGCAT-3')[49] were inserted into pRNAT-H1.1-shutter/GFP vector. To generate the pLVX-puro-ATP8A1-Flag plasmid, a Flag tag (DYKDDDDK) was inserted to the second extracellular loop (between Asn 331 and Leu 332) of ATP8A1 using the PCR overlap extension method, and the modified ATP8A1 was cloned into the pLVX-puro vector using PCR amplification and One Step Cloning Kit (Vazyme, Chnia). To construct lentiviral-based shATP8A1 and shATP11A plasmids, the nucleotide target sequence of the human ATP8A1 gene (5'-GCTATGGCTCGAACATCTA-3') or ATP11A gene (5'- GCTGCTGTTCTACGTTGTCTT-3') was inserted into the pLKO.1-puro lentiviral vector using AgeI/EcoRI sites. shRNA-resistant ATP8A1 was generated by introducing five silent mutations (T1167C, T1173G, A1176G, A1179G, T1182C) within the ATP8A1 shRNA target sequence (5'-GCTATGGCTCGAACATCTA-3').

ATP8A1E191Q mutant was constructed by site-directed mutagenesis of shRNA-resistant wild-type ATP8A1. Resulting plasmids were confirmed by DNA sequencing.

Generation of lentiviral-based stable cell lines

This study used the following stable cell lines: shATP8A1, shATP11A and ATP8A1-Flag. To obtain lentivirus plasmid system, HEK293T cells were transfected with recombinant pLKO.1-shATP8A1-puro or pLKO.1-shATP11A-puro or pLVX-ATP8A1-Flag-puro plasmids, along with lentiviral packaging vectors psPAX2 and pMD2.G. Lentivirus was harvested by taking media 48 h after transfection and filtered by 0.22 μm syringe filter. HeLa cells were infected with the collected lentiviral particles. After infection, selection was performed using 1 μg/ml of puromycin (Gibco, USA) for three days to obtain target cell lines.

Western blotting

For EGFR degradation or AKT/ERK phosphorylation assay, HeLa parental or ATP8A1-deficient stable cell lines were serum-starved in the absence or presence of BafA1 (500 nM) for 12 h, followed by treatment with 100 ng/ml EGF and 20 μg/ml cycloheximide at 37°C for the indicated times. At the end of the incubated time, total protein was extracted from cells using RIPA lysis buffer (Beyotime Biotechnology, China). Proteins were separated by SDS-PAGE and transferred to nitrocellulose membranes using a wet blot system (Bio-Rad, USA). The membranes were incubated with 1st and 2nd antibodies overnight at 4°C and 1h at room temperature (RT), respectively. The protein bands were visualized with Chemiluminescence (Thermo Fisher Scientific, UK) on the ChemiDocXRS + system (Bio-Rad, USA) and were quantified using ImageJ software.

Quantitative real-time polymerase chain reaction (qRT-PCR)

The knockdown efficiency of shRNA targeting ATP11A, ATP11C, ATP8A1 and CDC50A was identified at the mRNA level by qRT-PCR. Total RNA was extracted from cells using RNA-easy isolation reagent (Vazyme Biotech, China). Complementary DNA (cDNA) was synthesized from purified total RNA using Reverse Transcription Kit (Biosharp Life Science, China). qRT-PCR was conducted with SYBR Green PCR master mix (Vazyme Biotech, China) using Applied Biosystems QuantStudio 3 instrument and analyzed by QuantStudio™ Design & Analysis Software. Melting curve analysis was performed to ensure the production of a single amplicon. GAPDH was used as the internal control reference for the purpose of normalizing mRNA levels. The ΔΔCt method was used to determine relative mRNA expression.

Flow cytometry

HeLa cells stably expressing ATP8A1-Flag were trypsinized. For surface staining, cells were stained with anti-Flag rabbit antibody and Alexa Fluor 488 goat anti-rabbit antibody in DPBS for 30 min at 4°C, respectively, followed by twice wash in DPBS and fixed with Fixation solution (BD Biosciences, USA) for 20 min at 4°C. For intracellular staining, cells were fixed and permeabilized with Fixation/Permeabilization Solution (BD Biosciences) for 20 min at 4°C, followed by twice wash in Perm/Wash buffer (BD Biosciences, USA) and stained with 1st and 2nd antibodies diluted in Perm/Wash buffer for 30 min at 4°C, respectively.[50] Then cells were washed twice with Perm/Wash buffer, once with DPBS, and resuspended in DPBS. Fluorescence intensity (FI) of 10,000 cells per condition was measured on CytoFLEX flow cytometer (Beckman Coulter, USA) and analyzed using FlowJo software (Tree Star, USA).

Phosphatidylserine exposure on the plasma membrane was determined using Annexin V labeling. HeLa cells transfected with shcontrol, shATP11A, shATP11C or shATP8A1 were trypsinized, washed with ice-cold DPBS, and resuspended in 100 μl of 1 × binding buffer. Subsequently, cells were stained with 5 μl Annexin V FITC and 10 μl propidium iodide (Meilunbio, China) for 15 min at RT in dark. Reactions were stopped by adding 400 μl of 1 × binding buffer and cells were measured within 1 h by CytoFLEX flow cytometer. UV irradiation-induced apoptosis in HeLa cells were used as positive control (UV irradiation for 45 min).

Immunofluorescence

Cells on coverslips were fixed with 3.7% paraformaldehyde, blocked, and permeabilized with 2% BSA and 0.1% saponin, then incubated with 1st and 2nd antibodies for 45 min at RT, respectively. Nuclei were stained with DAPI for 10 min in the dark. Finally, coverslips were mounted on glass slides with 50% glycerol for image.

Confocal microscopy

Cells were visualized using a spinning-disk confocal system (CSU-X1 Nipkow; Yokogawa) equipped with an EM CCD camera (DU897K; ANDOR iXon) and oil objective lens (60 × N.A. 1.45 or 100 × N.A. 1.3). The laser included three channels: green (excitation 488 nm), red (excitation 561 nm), and blue (excitation 405 nm). Z-series of optical sections were obtained at 0.2 μm step size. Imaging settings (EM Gain and exposure time) were maintained consistent under the same experimental conditions.

Cargo proteins internalization and trafficking assay

Transferrin uptake and trafficking were followed. Cells on coverslip were allowed to internalize A568-Tfn (10 μg/ml) for 5 min at 37°C, followed by ice wash to remove the unbound A568-Tfn, and chase for indicated time periods in growth medium at 37°C. After ice wash, cells were fixed with 3.7% paraformaldehyde for 15 min and processed for imaging.

For surface EGFR trafficking assay, cells were serum-starved for 12 h before EGF (100 ng/ml) stimulation for indicated time periods at 37°C. EGFR internalization was stopped by replacing with ice-cold PBS before fixation with 3.7% paraformaldehyde for 15 min. The fixed cells were immune-stained with anti-EGFR rabbit antibody and Alexa Fluor 488 goat anti-rabbit antibody sequentially for imaging.

For M2 mAChR internalization assay, vehicle or shATP8A1 stable cells were co-transfected with EGFP-M2 and mCherry-Rab5Q79L, incubated with 100 μM carbachol in serum-free medium (α-MEM without phenol red supplemented with 20 mM Hepes pH 7.4 and 0.1% BSA) at 37°C for various time periods as indicated. Then, cells were washed extensively on ice with ice-cold serum-free medium thrice, fixed with 3.7% PFA for 15 min at room temperature.

Imaging analysis

Fluorescent images were analyzed with ImageJ software (Wayne Rasband, National Institutes of Health). Obtained image series were deconvolved with AutoQuant X2 software (Media Cybernetics, USA). To calculate the average FI of PM- or enlarged endosome-located signals, a line segment of 6- or 5-pixel-wide was drawn along the contour of the cell or endosomes using "Selection Brush Tool". Linear profile was performed to analyze pixel intensity of the line using ImageJ plugin "Plot Profile". Colocalization was reported as Pearson's coefficient calculated using ImageJ plugin "JACoP" on the basis of three independent experiments.[51] The scatter plot of the two channels showed the intensity correlation using Image J Colocalization Threshold.

To quantify Alexa555-EGF in the ILVs of Rab5Q79L-enlarged endosomes, a straight line was drawn across the diameter for each endosome, and pixel intensities of red channel along the line were measured. The average background fluorescence was subtracted from the raw pixel intensity values. To account for different endosome sizes, the pixel distance between the limiting membranes across the endosomal diameter was normalized (from 0 to 100). The pixel intensities along the drawn straight line across the diameter were also normalized through dividing by the maximal value of pixel intensities. The background-corrected and normalized pixel intensity values corresponding to pixels located 40-60% across the endosomal diameter were averaged and produced central luminal fluorescence values for each endosome.[52] The pixel intensities at the normalized position of 0 and 100 were considered as limiting membrane-located FI.

To quantify HRS foci or clathrin clusters or TSG101 foci decoration on the GFP-Rab5Q79L-labeled limiting membranes, a line was drawn along the contour length of enlarged endosomes using the tool "segmented line"; the pixel distance along the line was normalized (from 0 to 100). The pixel intensities of red channel along the line were measured and normalized according to the formula $(FI-FI_{min})/(FI_{max}-FI_{min})$, in which FI_{max} and FI_{min} represent the maximal and minimal pixel intensities across the line, respectively. Pixels with normalized intensity exceeding 0.2 or 0.3 were counted as HRS-/clathrin-/TSG101-occupied limiting membrane contour, which were summed and expressed as the percentage of the total limiting membrane length.

QUANTIFICATION AND STATISTICAL ANALYSIS

The statistical analyses were conducted employing the GraphPad Prism software verdsion 8.0 (San Diego, USA). Datasets were checked for normalcy with Shapiro-Wilk test and then chose appropriate test accordingly. For datasets of nonnormal distribution, Mann-Whitney test were used to compare two groups, or Kruskal-Wallis test to compare multiple groups. For datasets of normal distribution, unpaired two-tailed Student's t test were used to compare two groups, or one-way ANOVA with Tukey's post hoc test to compare multiple groups. All experiments were performed independently at least three times. The data are presented as mean ± SEM or mean ± SD. A p value < 0.05 ($p < 0.05$) was considered to be statistically significant when $^{*}p < 0.05$, $^{**}p < 0.01$, $^{***}p < 0.001$, $^{****}p < 0.0001$, ns = not significant, $p > 0.05$.